A boost to Higgs Physics: new regimes at high energy

Silvia Biondi
University & INFN of Bologna
silvia.biondi@cern.ch / silvia.biondi@bo.infn.it

Corso di Dottorato - 2019/2020

Course outline

- Theory reminder
- Higgs boson production and decay modes
- Higgs boson discovery by ATLAS and CMS
- **Higgs boson mass measurement by ATLAS and CMS**
- **Overview of ATLAS and CMS analyses about Higgs**
- Signal/background discrimination techniques
  - boosted regimes
    - tagging, large-radius jets substructure, re-clustering
  - multivariate analysis and deep neural network
- Signal extraction techniques
  - likelihood and test statistic
  - CLs method
- ttH analysis: an example

Higgs boson: mass measurement

Higgs boson mass measurement: strategy

☆ [Combined Measurement of the Higgs Boson Mass in pp Collisions at √s=7 and 8 TeV with the ATLAS and CMS Experiments]

Why it's important:

- With m_H known, **all properties of the SM Higgs boson**, such as its production cross section and partial decay widths, **can be predicted**;
- Increasingly precise measurements have established that **all observed properties of the new particle**, including its spin, parity, and coupling strengths to SM particles are **consistent within the uncertainties with those expected for the SM Higgs boson**.

$$H \to \gamma\gamma$$

Strategy:

- CMS uses the same analysis procedure for the measurement of the Higgs boson mass and couplings
- ATLAS implements separate analyses for the couplings and for the mass:
  - classifies events in a manner that reduces the expected systematic uncertainties in m_H.

↓

- **narrow resonant signal peak with several hundred events** per experiment above a large continuum background;
- different categories depending on the signal purity and mass resolution to improve sensitivity.

$$H \to ZZ^* \to 4l$$

Strategy:

- CMS uses a three-dimensional fit, utilising the four-lepton mass distribution, a kinematic discriminant, and the estimated event-by-event uncertainty in the four-lepton mass;
- ATLAS employs a two-dimensional (2D) fit to the distribution of the four-lepton mass and a kinematic discriminant introduced to reject the main background.

↓

- **only a few tens of signal events** per experiment, but very little background;
- events are analysed separately depending on the flavour of the lepton pairs.

Higgs boson mass measurement: statistical analysis

NB!!

- only minor differences in the parameterisations used for the present combination compared to those used for the combination of the two channels by the individual experiments;
- almost no effect on the results.

⭐ **Maximisation of the profile-likelihood ratios:**

$$\Lambda(\alpha) = \frac{L(\alpha, \hat{\hat{\theta}}(\alpha))}{L(\hat{\alpha}, \hat{\theta})}$$

α = parameters of interest
θ = nuisance parameters NPs (those corresponding to systematic uncertainties, the fitted parameters of the background models, and any unconstrained signal model parameters not relevant to the particular hypothesis under test)
$\hat{\alpha}, \hat{\theta}$ = unconditional maximum likelihood estimates of the best-fit values for the parameters
$\hat{\hat{\theta}}$ = conditional maximum likelihood estimate for given parameter values a.

constructed using signal and background probability density functions (PDFs) that depend on the discriminating variables:

$H \rightarrow \gamma\gamma$

diphoton invariant mass

- signal PDFs: derived from MC samples;
- background PDFs: obtained directly from the fit to the data.

$H \rightarrow ZZ^* \rightarrow 4l$

four-lepton invariant mass

- signal PDFs: derived from MC samples;
- background PDFs: combination of MC and data control regions.

Important to perform a mass measurement that is as independent as possible of SM assumptions

- three signal-strength scale factors: reducing the dependence of the results on assumptions about the Higgs boson couplings and about the variation of the σxBR with the mass;

$\mu^{\gamma\gamma}_{\mathbf{ggF+t\bar{t}H}}$ $\mu^{\gamma\gamma}_{\mathbf{VBF+VH}}$ $\mu^{\mathbf{4l}}$

Higgs boson mass measurement: results

- **Profile-likelihood fits to the data** are performed as a function of m_H and the signal-strengths ($\mu^{\gamma\gamma}_{ggF+t\bar{t}H}$, $\mu^{\gamma\gamma}_{VBF+VH}$, μ^{4l});
- **statistical uncertainty** determined by fixing all nuisance parameters to their best-fit values, except for the three signal-strength scale factors and the H → γγ background function parameters, which are profiled;
- **systematic uncertainty** determined by subtracting in quadrature the statistical uncertainty from the total uncertainty.

combined overall signal strength: $\mu = 1.24^{+0.18}_{-0.16}$

m_H = 125.09 ± 0.24 GeV = 125.09 ± 0.21 (stat) ± 0.11 (sys) GeV

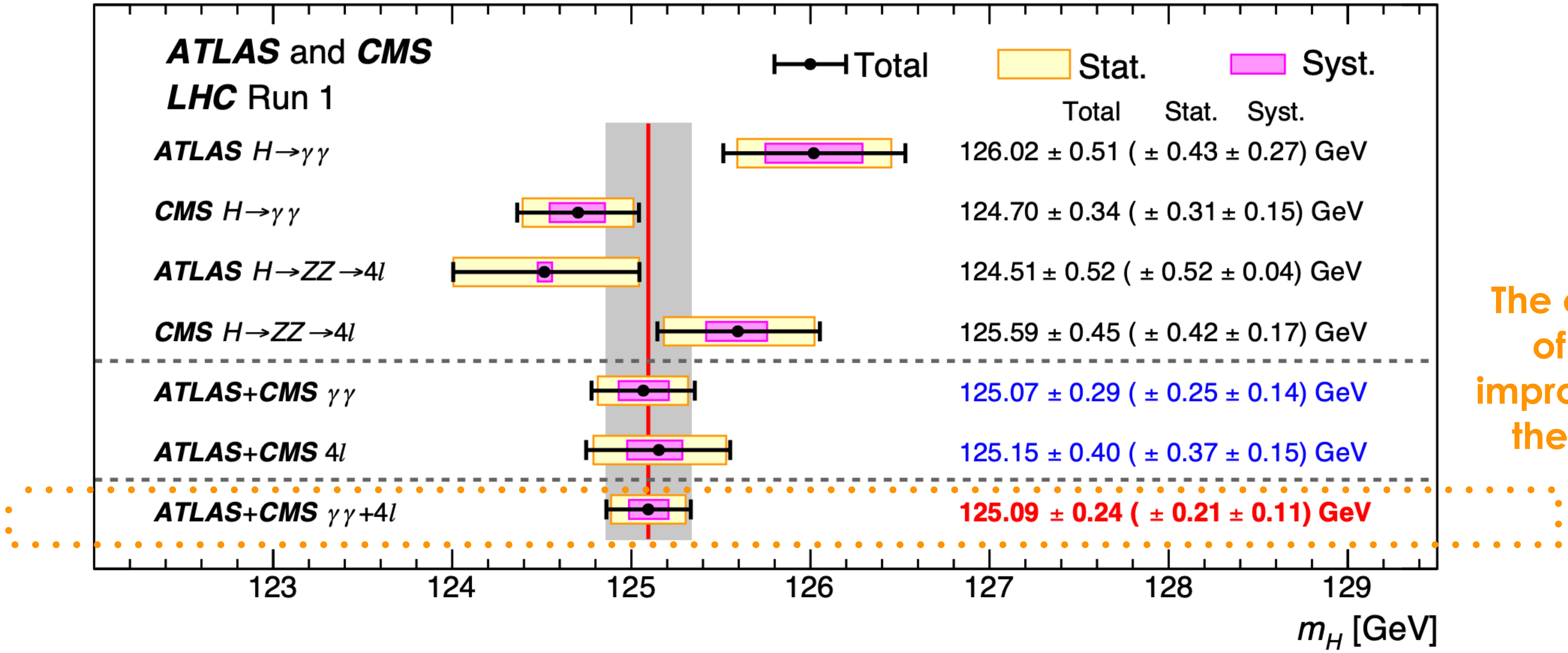

The combined measurement of the Higgs boson mass improves upon the results from the individual experiments

Higgs boson mass measurement: results

Results interpretation

- **Compatibility of the signal strengths from ATLAS and CMS** is evaluated through:

$\lambda^{\mathrm{expt}} = \mu^{\mathrm{ATLAS}}/\mu^{\mathrm{CMS}}$ $\quad \lambda_{\mathrm{F}}^{\mathrm{expt}} = \mu_{\mathrm{ggF+t\bar{t}H}}^{\gamma\gamma\,\mathrm{ATLAS}}/\mu_{\mathrm{ggF+t\bar{t}H}}^{\gamma\gamma\,\mathrm{CMS}}$ $\quad \lambda_{\mathrm{4l}}^{\mathrm{expt}} = \mu^{\mathrm{4l\,ATLAS}}/\mu^{\mathrm{4l\,CMS}}$

- each ratio individually taken to be the parameter of interest, with all other NPs profiled, including the remaining two ratios for the first two tests.

$\lambda^{\mathrm{expt}} = 1.21^{+0.30}_{-0.24}$

$\lambda_{\mathrm{F}}^{\mathrm{expt}} = 1.3^{+0.8}_{-0.5}$ **all consistent with unity within 1 σ**

$\lambda_{\mathrm{4l}}^{\mathrm{expt}} = 1.3^{+0.5}_{-0.4}$

- **Correlation between the signal strength and the measured mass** is explored with 2D likelihood scans as functions of μ and m_H.
- The three signal strengths are assumed to be the same:

$$\mu_{\mathrm{ggF+t\bar{t}H}}^{\gamma\gamma} = \mu_{\mathrm{VBF+VH}}^{\gamma\gamma} = \mu^{\mathrm{4l}} = \mu$$

- the ratios of the $\sigma_{\mathrm{prod}} \times \mathrm{BR}$ are constrained to the SM predictions.
- Assuming that the negative log-likelihood ratio $-2\ln\Lambda(\mu, \mathrm{m_H})$ is distributed as a χ^2 variable with two degrees of freedom, the 68% confidence level (CL) confidence regions are shown.

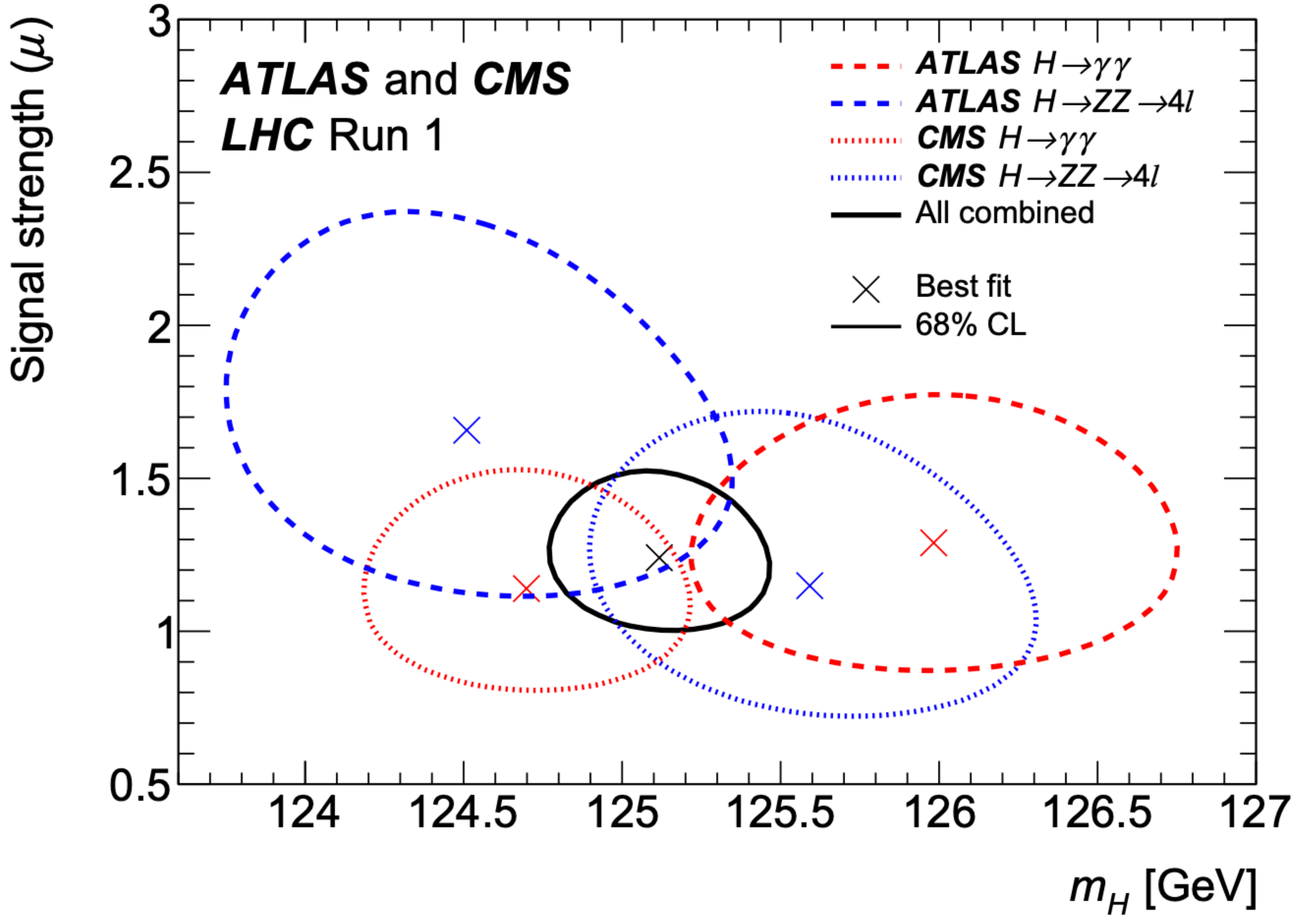

Higgs boson mass measurement: systematic uncertainties

Treatment and understanding of systematic uncertainties is an important aspect of the individual measurements and their combination:

- **~ 300 NPs**: ~100 fitted parameters describing the shapes and normalisations of the background models in the H → γγ channel;
- remaining ~ almost 200 NPs, most correspond to experimental or theoretical systematic uncertainties.

How to treat them:

- impact of groups of NPs is evaluated starting from the **contribution of each individual NP to the total uncertainty**:
  - defined as the **mass shift δm_H** observed when re-evaluating the profile-likelihood ratio after fixing the NP in question to its best-fit value increased or decreased by 1 standard deviation (σ) in its distribution;
- **impact of a group of NPs** is estimated by summing in quadrature the contributions from the individual parameters.

The largest systematic effects are related to the determination of the energy scale of the photons, followed by those associated with the determination of the electron and muon momentum scales.

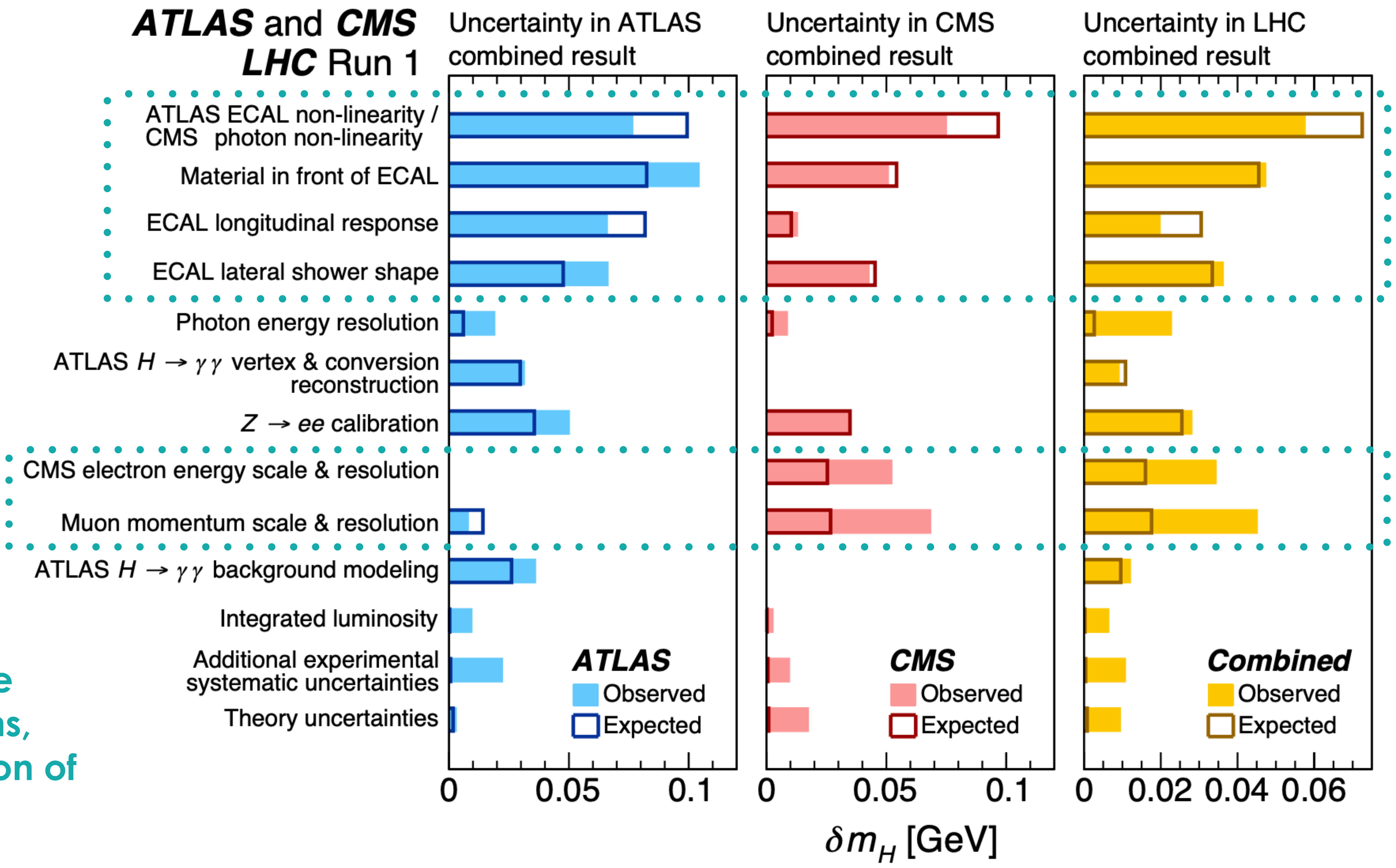

Overview of ATLAS and CMS analyses about Higgs

Higgs boson story at the LHC

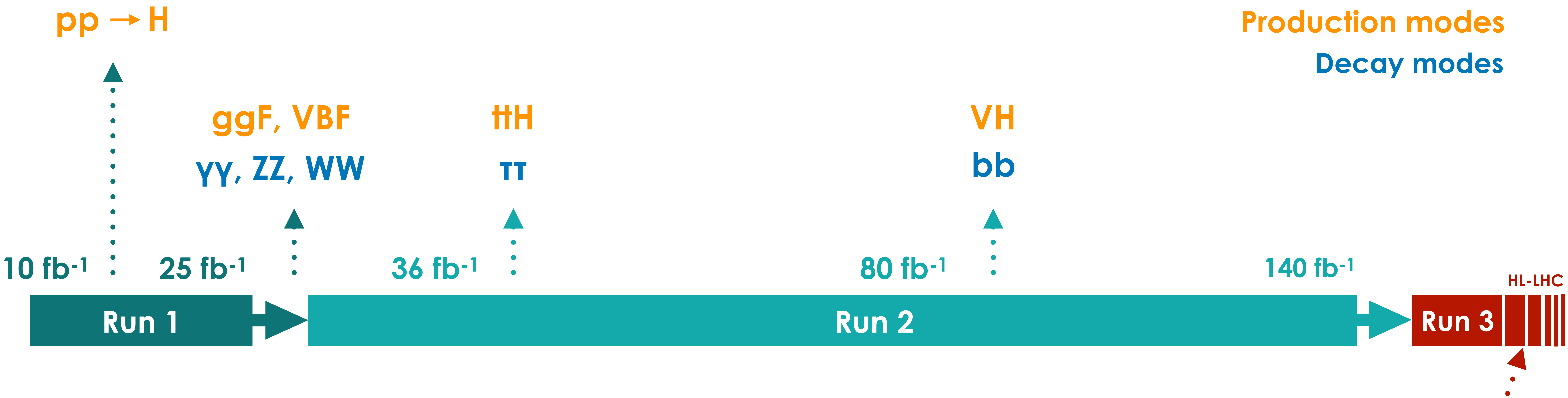

Rare productions and decays?

Precision measurements of the properties of the Higgs boson are an important test of the SM

- **Yukawa coupling strengths** are free parameters in the SM and do not explain the observed pattern of fermion masses;
- not understood why the Higgs boson mass is near the **electroweak scale**, since it is not protected in the SM from large quantum corrections;
- development of many beyond the SM (**BSM**) theories that can alter the properties of the Higgs boson.

Properties:
- mass
- spin and parity
- couplings
- width
- lifetime

Measurements:
- inclusive cross-section
- differential cross-section
- Simplified Template X-Section

Higgs boson mass measurement: new results

PLB 784 (2018) 345

ATLAS

25 fb^{-1}+36 fb^{-1}

$H \rightarrow ZZ^* \rightarrow 4l$

$H \rightarrow \gamma\gamma$

Strategy H → ZZ → 4l:
- similar to H→4l analysis:
  - **110 < m_{4l} < 135 GeV**;
  - **4 categories**: 4e, 2e2μ, 2μ2e and 4μ

Strategy H → γγ:
- more complex wrt H→γγ analysis:
  - **105 < $m_{\gamma\gamma}$ < 160 GeV**;
  - **31 categories** split in terms of jets, production modes, etc

- maximisation of the profile-likelihood ratio;
- Likelihood based on Higgs mass;
- **combination with Run 1 data** (7-8 TeV, 25 fb^{-1})

m_H = 124.97 ± 0.19 (stat) ± 0.13 (sys) GeV

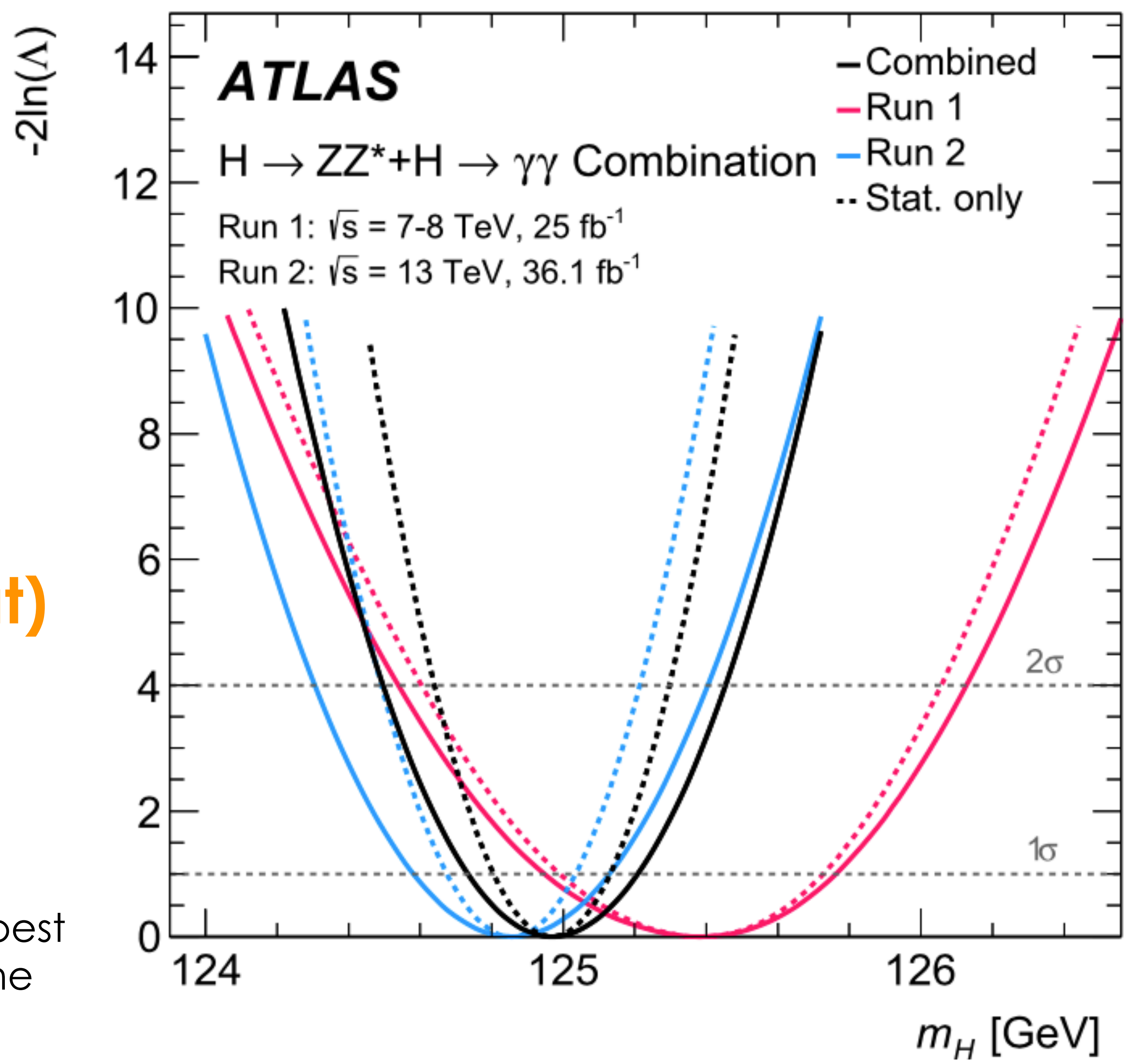

* generated from the likelihood distribution Λ with NPs fixed at the best fit value obtained on data and the POI fixed to SM hypothesis

35.9 fb^{-1}

CMS

JHEP 11 (2017) 047

$H \rightarrow ZZ^* \rightarrow 4l$

Strategy:
- more complex wrt previous H→4l analysis:
  - **118 < m_{4l} < 130 GeV**;
  - event categorisation to enhance the signal purity based on production modes;
  - **3 categories**: 4e, 2e2μ and 4μ

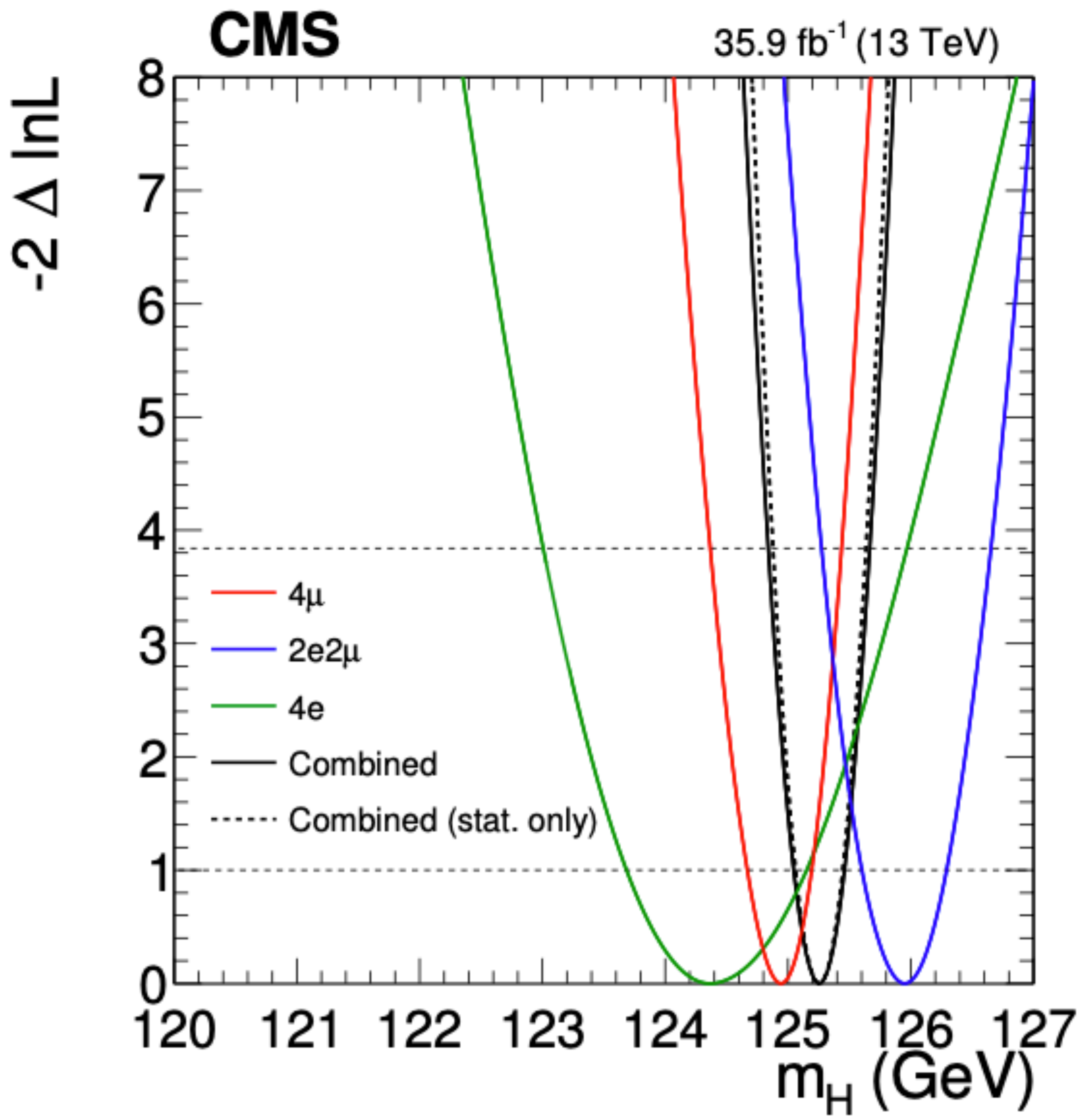

- maximisation of the profile-likelihood ratio;
- Likelihood based on Higgs and Z mass, leptons p_T and invariant mass.

m_H = 125.26 ± 0.20 (stat) ± 0.08 (sys) GeV

* generated from the likelihood distribution Λ with NPs fixed at the best fit value obtained on data and the POI fixed to SM hypothesis

Higgs boson cross-section measurement: inclusive

PRD 101 (2020) 012002 — **ATLAS** — $H \to \gamma\gamma, ZZ^*, WW^*, \tau\tau, b\bar{b}, \mu\mu$ — **CMS** — EPJC 79 (2019) 421

ATLAS: up to 79.8 fb^{-1} — CMS: 35.9 fb^{-1}

Strategy

- **each analysis performed independently** with many event categories:
  - more than 60 categories per experiment;
- likelihood function defined as the product of the likelihoods of each input analysis;
- **simultaneous fit to data**, with xsec of each processes as POI;
- measurement of the **signal strength of the Higgs production process**.

$$\mu = \frac{\sigma_{\text{observed}}}{\sigma_{\text{SM}}}$$

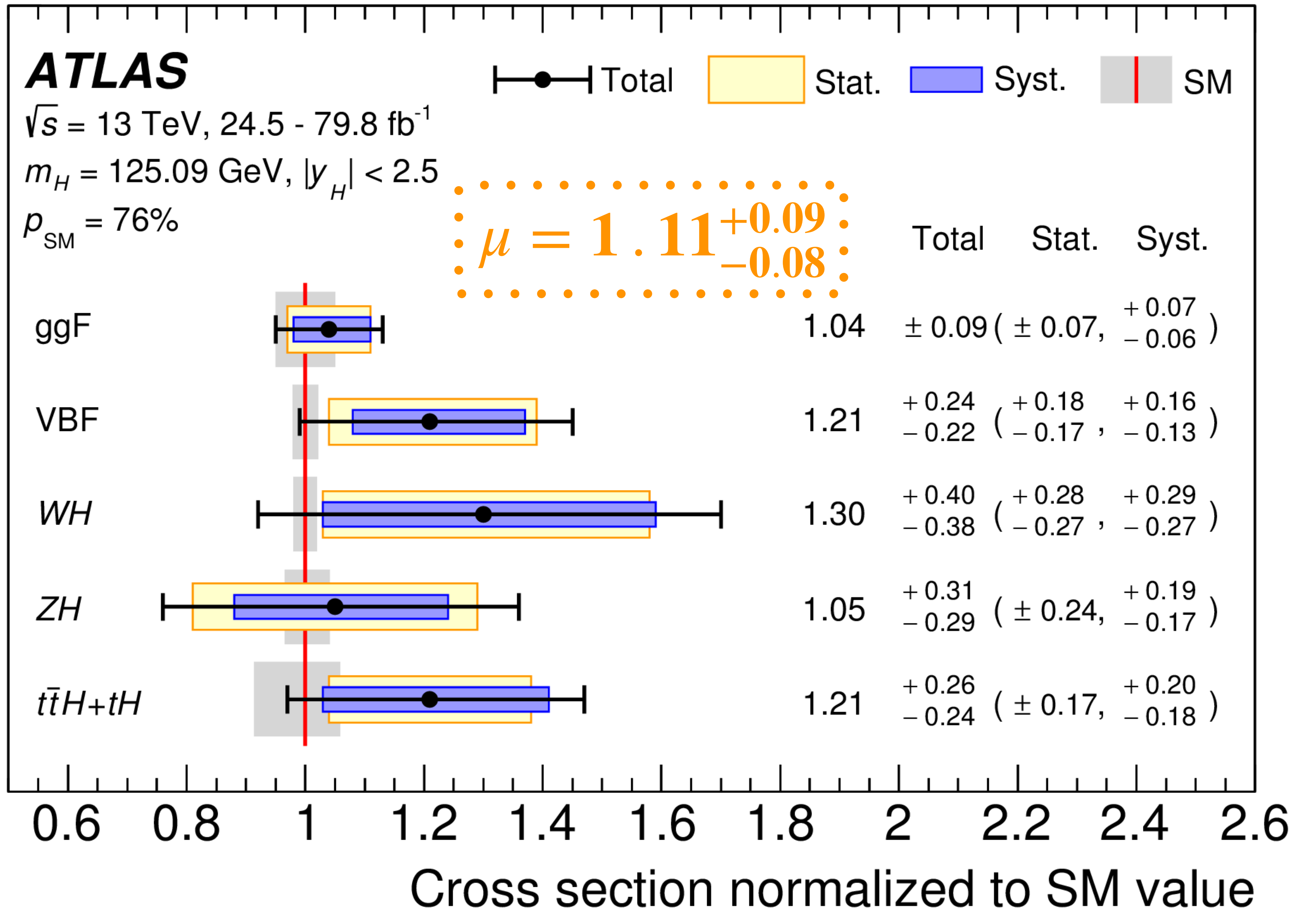

Systematic uncertainties treatment

- systematic uncertainties affecting multiple analyses are modelled with common NPs;
- **experimental uncertainties** treated as uncorrelated;
- **theory uncertainties in the signal** (QCD corrections and PFD choice) affect the exp. signal yields of each production and decay process
  - modelled by a common set of NPs;
- **background modelling uncertainties** treated as uncorrelated.

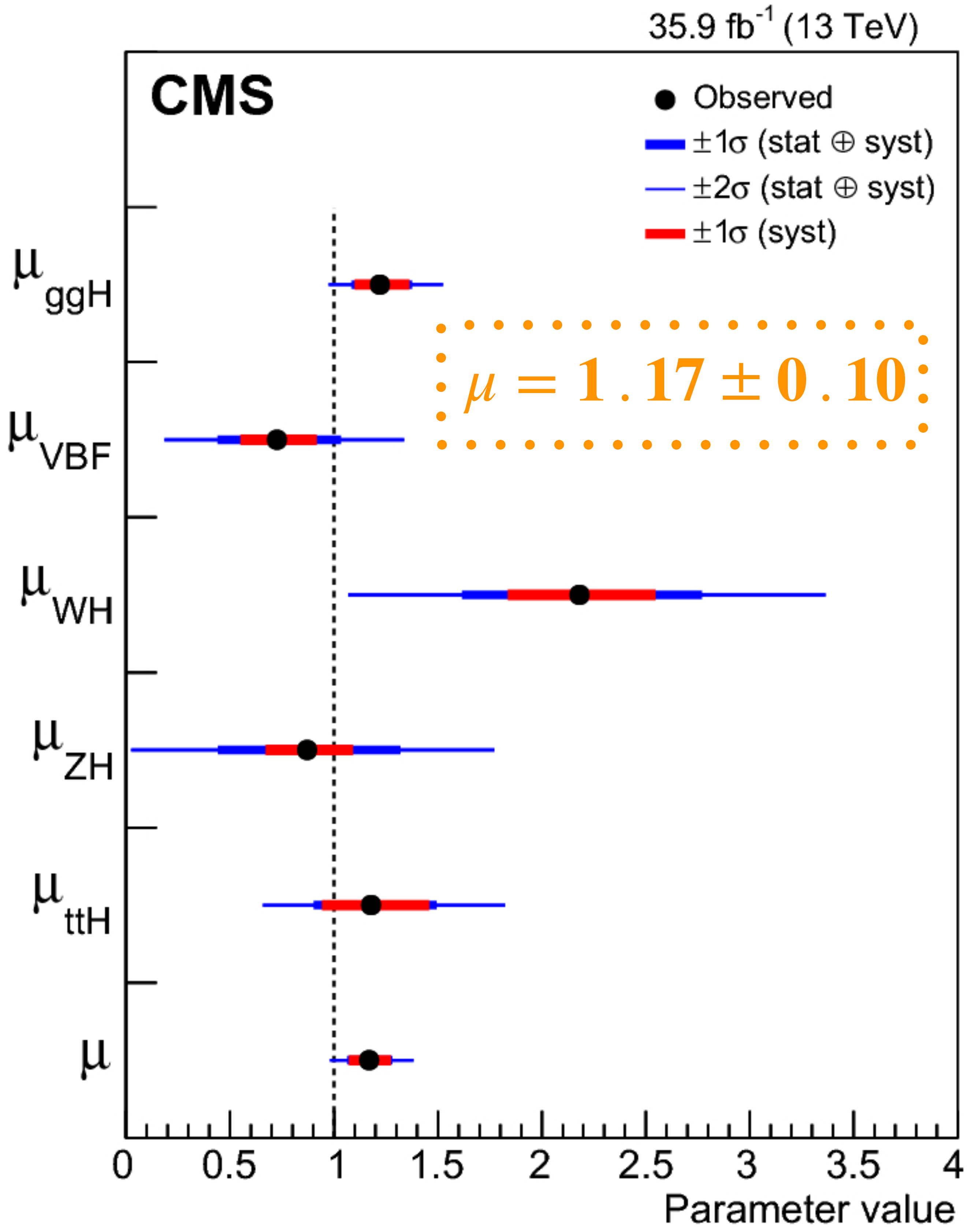

Higgs boson cross-section measurement: inclusive

PRD 101 (2020) 012002 **ATLAS** $H \to \gamma\gamma, ZZ^*, WW^*, \tau\tau, b\bar{b}, \mu\mu$ **CMS** EPJC 79 (2019) 421

up to 79.8 fb^{-1} **35.9 fb^{-1}**

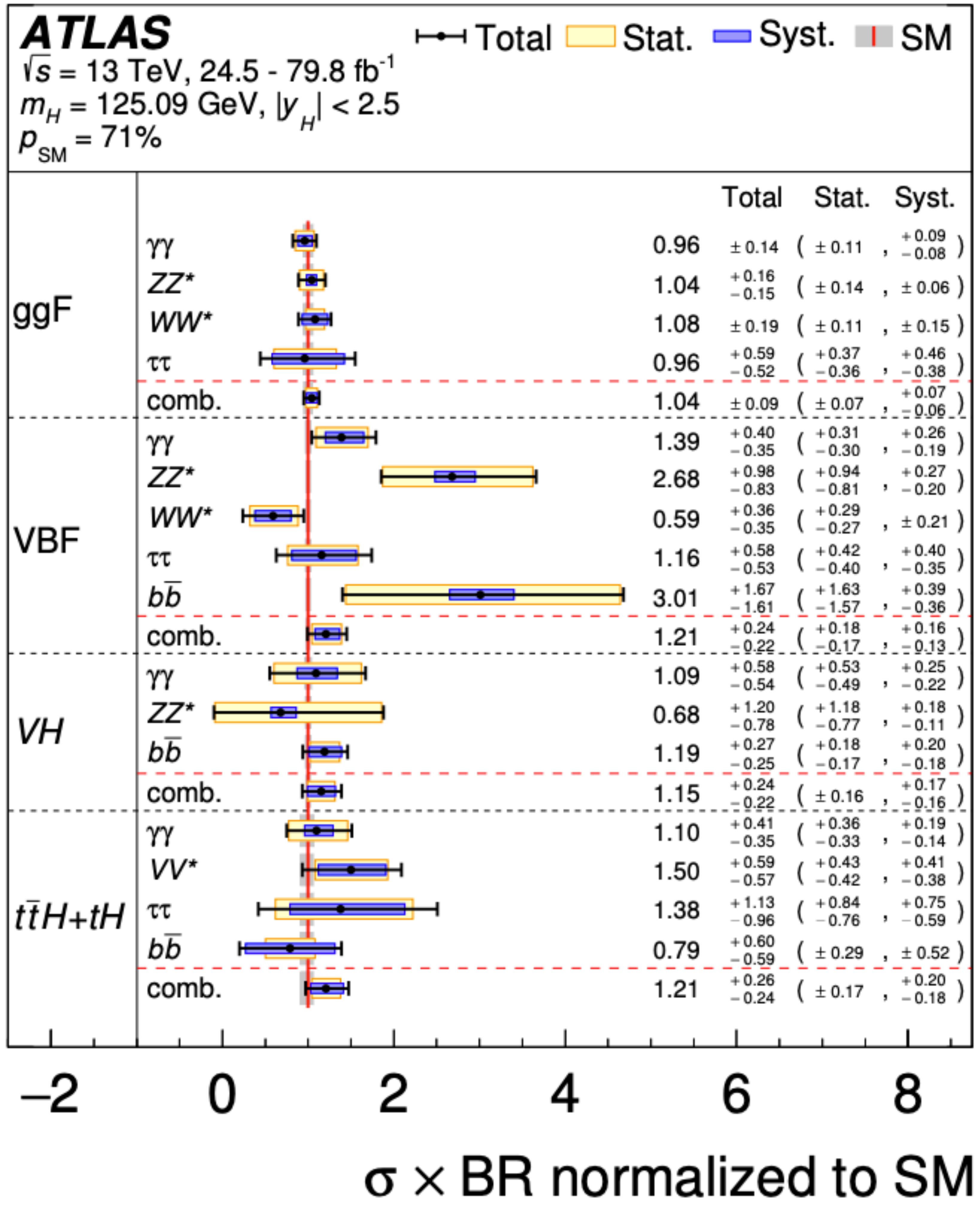

Products of cross sections and BRs

- A **description of both the production and decay mechanisms of the Higgs boson** is obtained by considering the products $\sigma_{\text{prod}} \times \text{BR}$ of the cross section in production process *i* and branching fraction to final state *f*.

$$\mu_{\text{if}} = \frac{\sigma_{\text{i}}}{\sigma_{\text{i}}^{\text{SM}}} \times \frac{\text{BR}_{\text{f}}}{\text{BR}_{\text{f}}^{\text{SM}}}$$

- **Not all the processes are considered** (VH→ττ for both, VBF→bb for CMS), due to low sensitivity;
- CMS restricts to non-negative values some signal strengths
  - background contamination is sufficiently low so that a negative signal strength can result in an overall negative event yield.

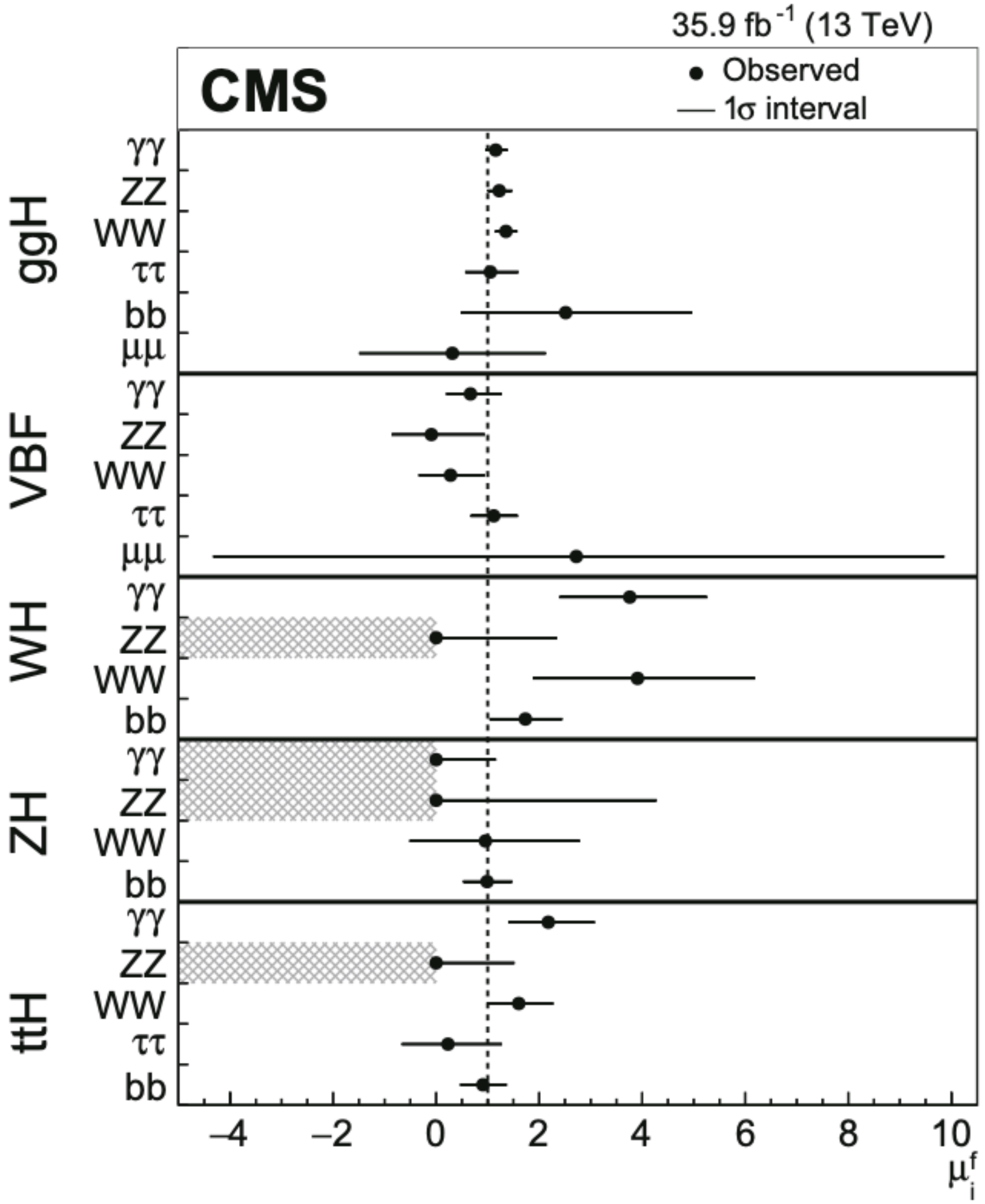

Higgs boson couplings: combined measurement

PRD 101 (2020) 012002 **ATLAS** $H \to \gamma\gamma, ZZ^*, WW^*, \tau\tau, b\bar{b}, \mu\mu$ **CMS** EPJC 79 (2019) 421

up to 79.8 fb^{-1} **35.9 fb^{-1}**

κ- framework model to study Higgs couplings

- assumed that there are **no BSM contributions to the total Higgs boson width**;
- coupling modifiers are introduced in order to **test for deviations in the couplings of the Higgs boson to other particles**;
- for a given production process or decay mode *j*, a coupling modifier κ_j is defined such that $\kappa_j^2 = \sigma_j/\sigma_j^{SM}$ or $\kappa_j^2 = \Gamma_j/\Gamma_j^{SM}$
- Individual coupling modifiers, corresponding to tree-level Higgs boson couplings to the different particles, are introduced.

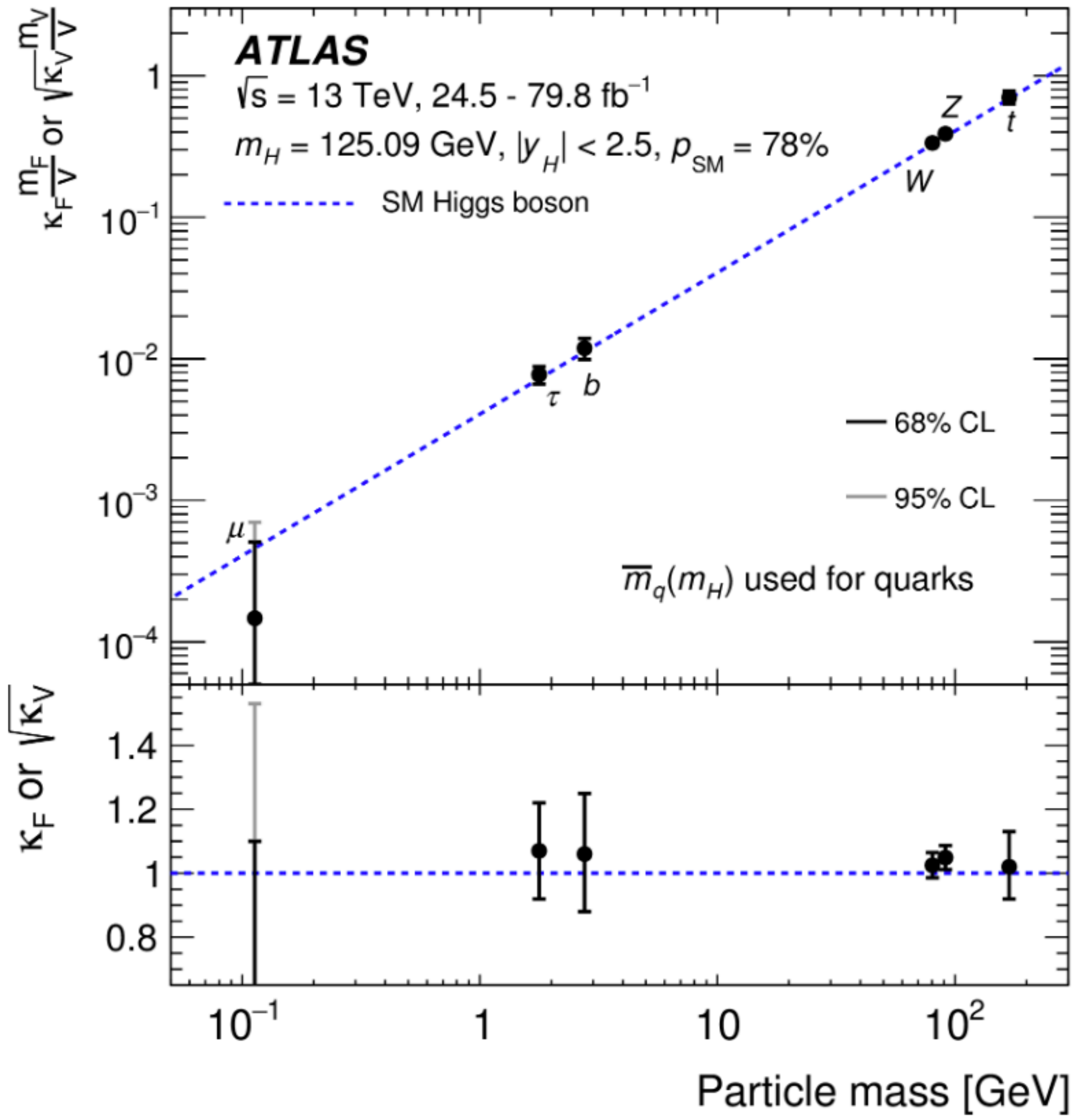

Results in terms of reduced coupling-strength scale factors

- $y_V = \sqrt{\kappa_V}\frac{m_V}{v}$

  for weak bosons with a mass m_V

- $y_F = \kappa_F\frac{m_F}{v}$

  for fermions with a mass m_F.

* **v** = 246 GeV

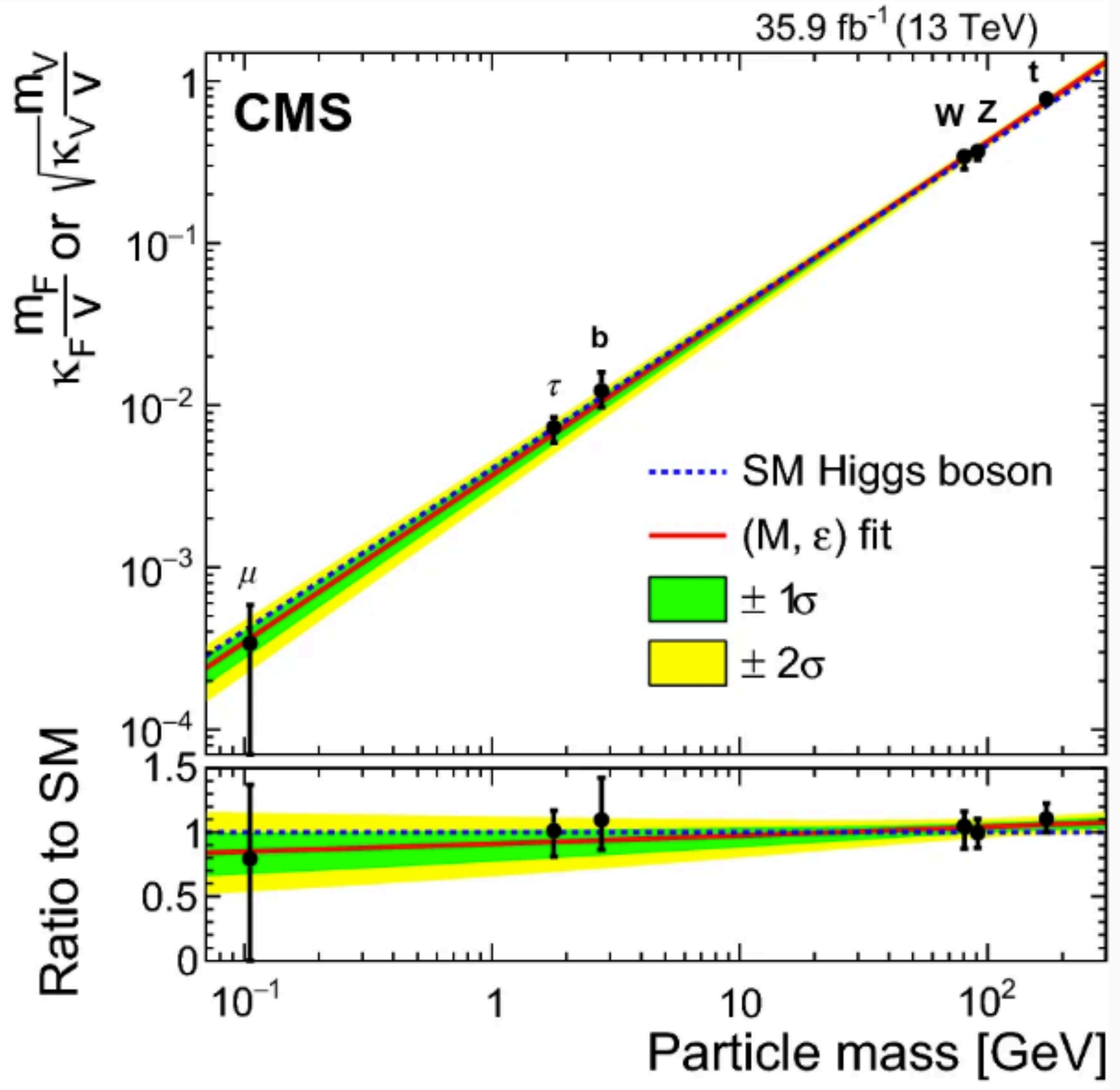

Higgs boson couplings: combined measurement

PRD 101 (2020) 012002 — **ATLAS** — up to 79.8 fb^{-1}

$H \rightarrow \gamma\gamma, ZZ^*, WW^*, \tau\tau, b\bar{b}, \mu\mu$

CMS — 35.9 fb^{-1} — EPJC 79 (2019) 421

Probing the universal coupling-strength scale factors

- $\kappa_V = \kappa_W = \kappa_Z$ and $\kappa_F = \kappa_t = \kappa_b = \kappa_\tau = \kappa_\mu$
- **presence of any BSM particles is not expected to significantly change the corresponding kinematic properties of the processes**
  - no invisible or undetected Higgs boson decays, i.e. $B_{inv} = B_{undet} = 0$;
  - only the relative sign between κ_V and κ_F is physical.

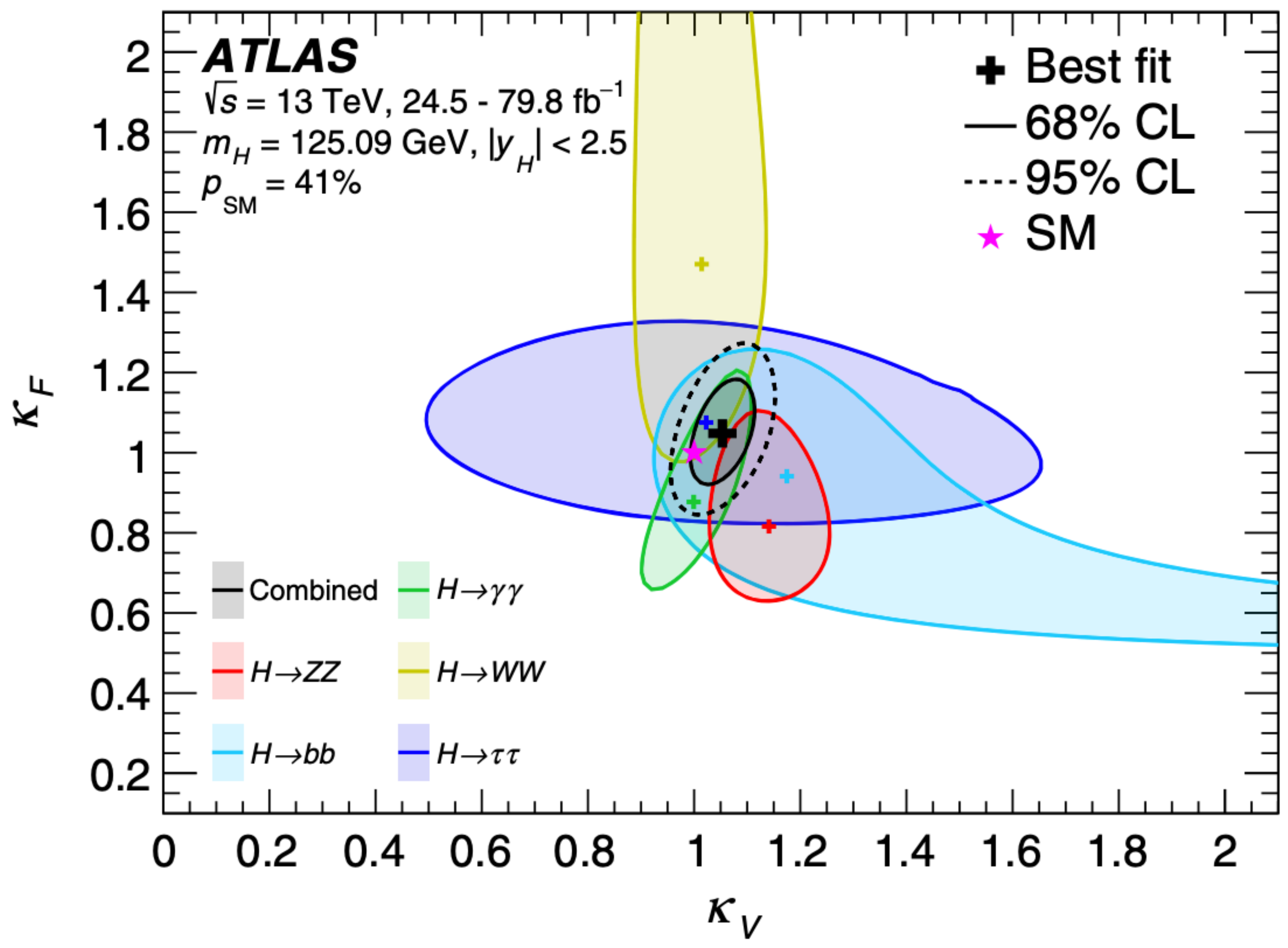

Results of the combined fit in the (κ_V, κ_F) plane as well as those of the individual decay modes in this benchmark model.

Both κ_V and κ_F are measured to be compatible with the SM expectation.

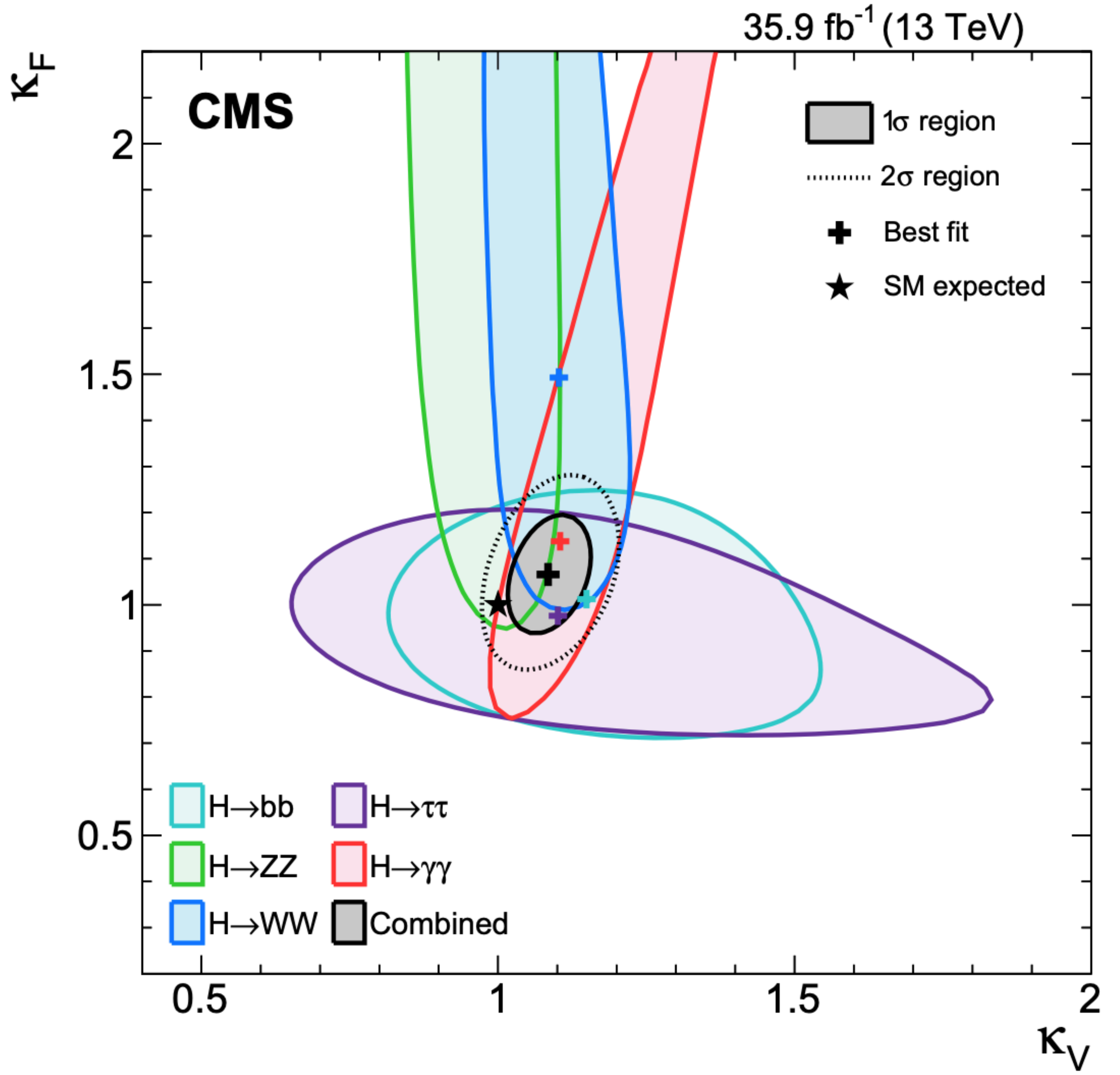

Higgs boson cross-section measurement: differential

ATLAS-CONF-2019-032 | **ATLAS** $H \to \gamma\gamma, ZZ^*$ | 139 fb^{-1}

35.9 fb^{-1} | **CMS** $H \to \gamma\gamma, ZZ^*, b\bar{b}$ | PLB 792 (2019) 369

Differential Higgs boson production cross sections are sensitive probes for physics beyond the SM!

- it may manifest itself through **deviations from the distributions predicted by the SM**;
- xsec measured as a **function of interesting observables**, different bins defined;
- **fiducial phase spaces** defined at particle level that resemble the detector acceptance and analysis selections;
- the measured cross sections are model independent and are compared with predictions of various QCD calculations

Higgs p_T, Higgs rapidity ($H\to\gamma\gamma$ only)

- Experimental and theoretical uncertainties affecting both channels are correlated (common NPs);
- uncertainties in acceptance and correction factors (due to parton shower variations) are correlated;
- all the other are uncorrelated.

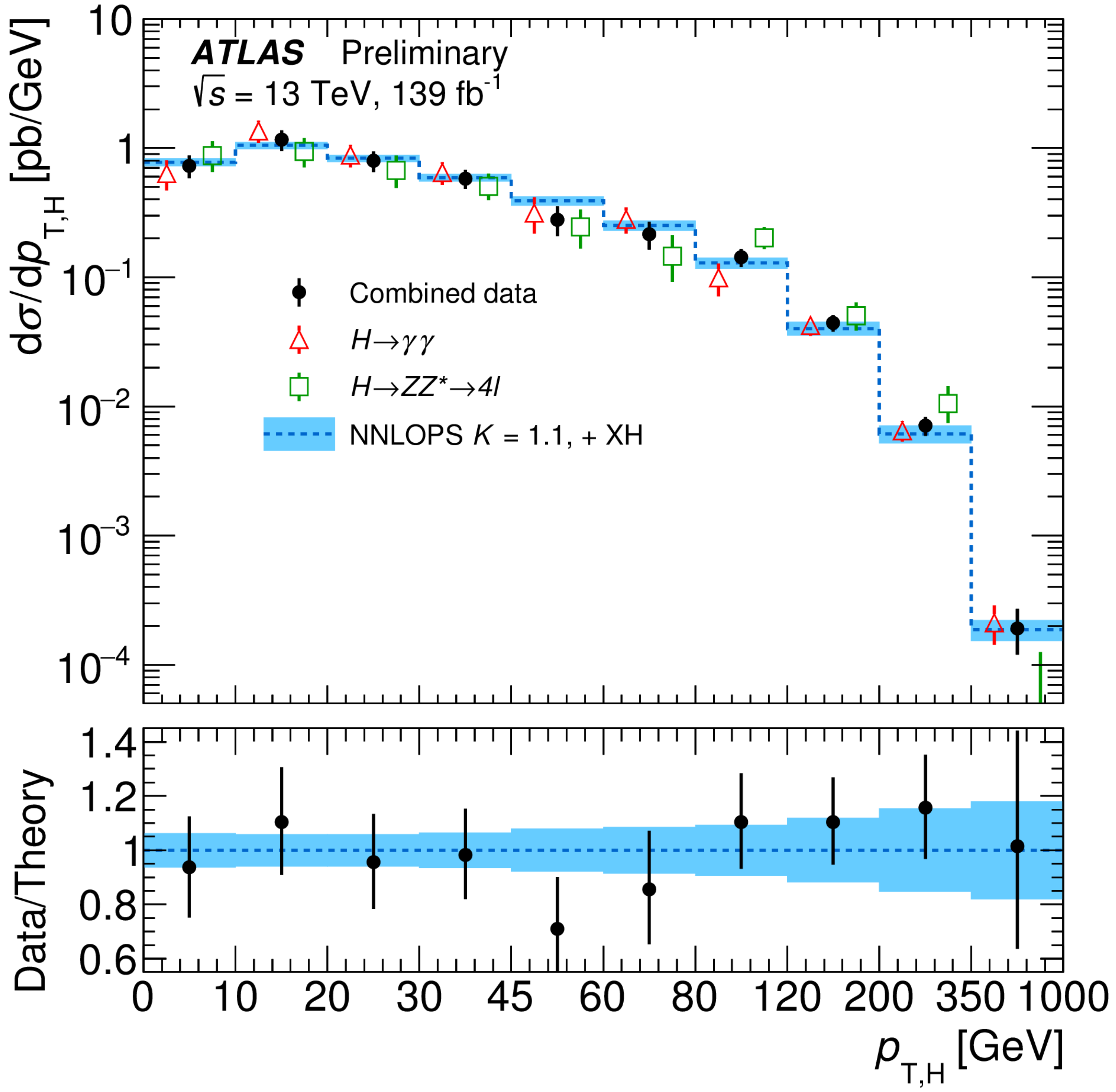

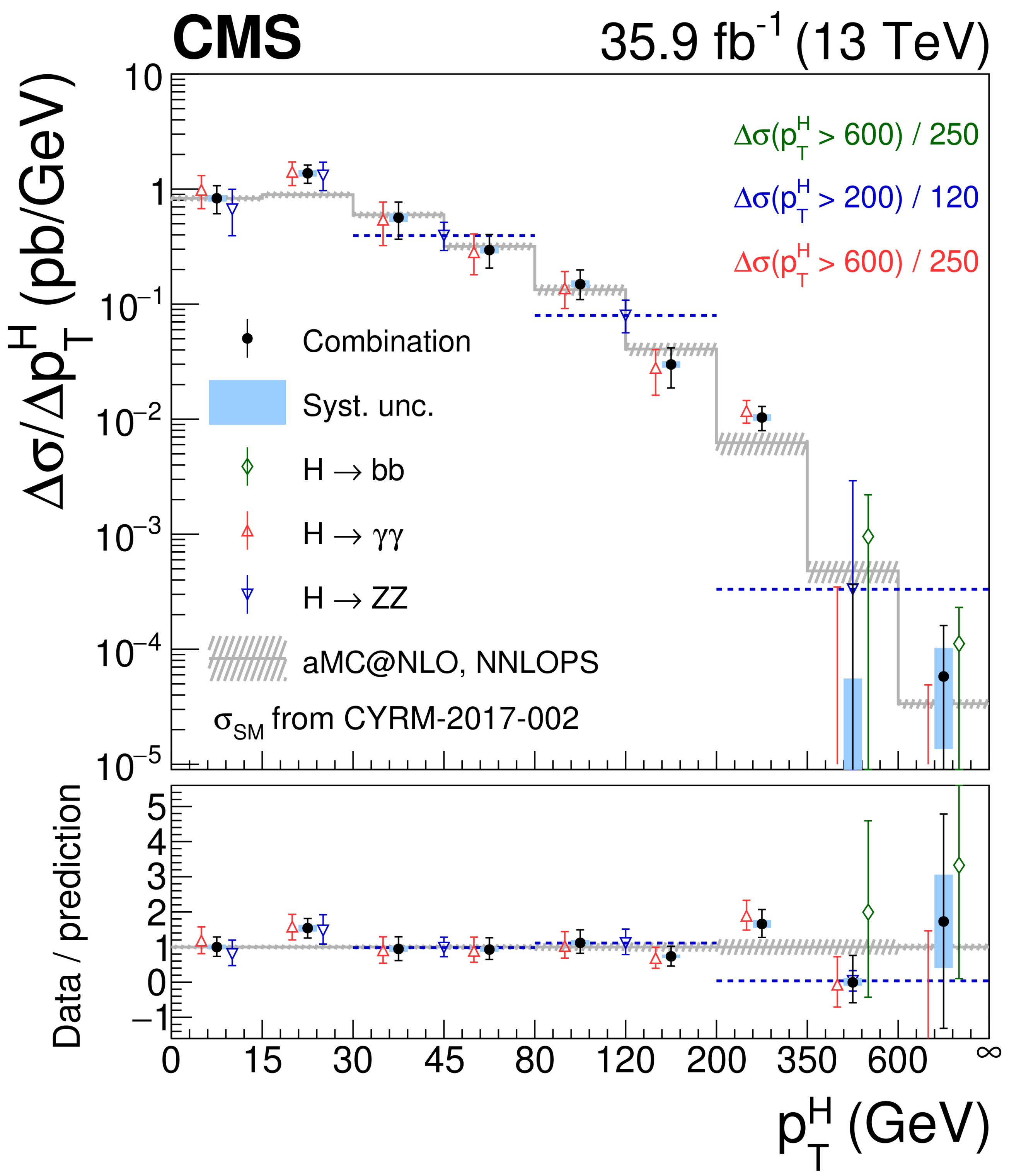

Higgs p_T, jet multiplicity, Higgs rapidity, jet p_T

- $H\to bb$ included only in the combination of the Higgs p_T spectra;
- experimental syst uncertainties from the input analyses are incorporated in the combination as NPs in the extended likelihood fit and are profiled;
- theory uncertainties subject to bin-to-bin correlations.

Higgs boson cross-section measurement: differential

ATLAS-CONF-2019-032 **ATLAS** $H \to \gamma\gamma, ZZ^*$

139 fb^{-1} 35.9 fb^{-1}

CMS $H \to \gamma\gamma, ZZ^*, b\bar{b}$ PLB 792 (2019) 369

Total cross-section measurement

- H→γγ and H→ZZ only for both the experiments;
- both the results are in good agreement with SM prediction ($\sigma_{TOT}^{SM} = 55.6 \pm 2.5$ pb).

$$\sigma_{TOT} = 55.4 \pm 3.1\,(\text{stat})\,^{+3.0}_{-2.8}\,(\text{syst})\ \text{pb}$$

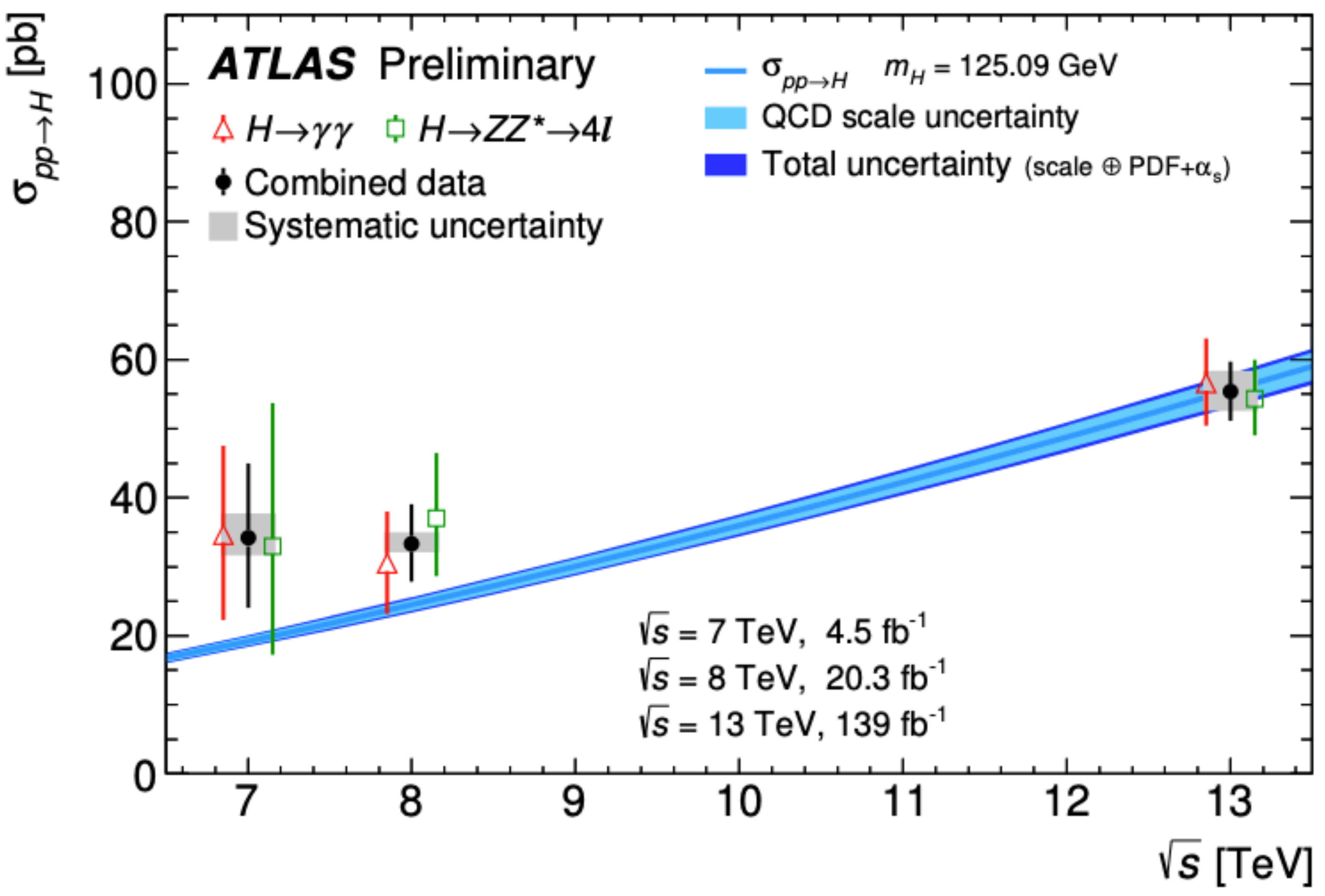

$\sigma_{H\to\gamma\gamma} = 56.7^{+6.4}_{-6.2}$ pb

$\sigma_{H\to ZZ} = 54.4^{+5.6}_{-5.4}$ pb

- combination improves the precision by ~20% wrt the H→γγ channel individually

$$\sigma_{TOT} = 61.1 \pm 6.0\,(\text{stat}) \pm 3.7\,(\text{syst})\ \text{pb}$$

$\sigma_{H\to\gamma\gamma} = 64.0 \pm 9.6$ pb

$\sigma_{H\to ZZ} = 58.2 \pm 9.8$ pb

- combination improves the precision by 27% wrt the H→γγ channel individually

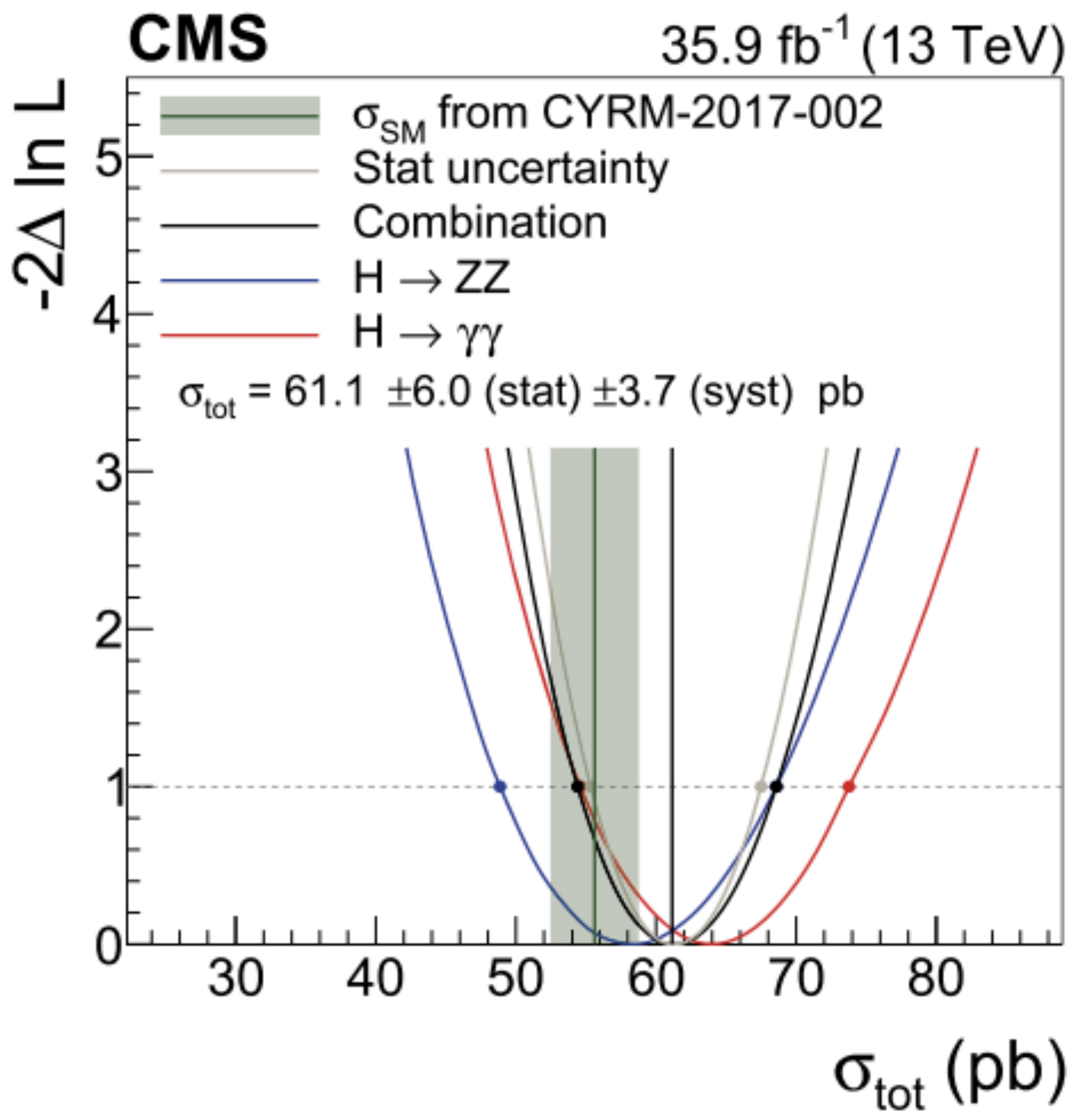

Higgs boson width measurement: constraints

PLB 786 (2018) 223-244 — **ATLAS** — 36 fb^{-1}

$H \to ZZ^* \to 4l/2l2\nu$ $\quad H \to ZZ \to 4l/2l2\nu$

CMS — 24.8 fb^{-1}+80.2 fb^{-1} — JHEP 11 (2017) 047

$H \to ZZ^* \to 4l$ $\quad H \to ZZ \to 4l$

Combination of on-shell and off-shell analyses:

- **non negligible interference effects** between the production processes;
- measurement of the relative off-shell and on-shell event yields provides **direct information about** Γ_H

$$\mu_{\text{off-shell}} = \frac{\sigma^{gg\to H^*\to ZZ}_{\text{off-shell}}}{\sigma^{gg\to H^*\to ZZ}_{\text{off-shell, SM}}} = k^2_{\text{g, off-shell}} \cdot k^2_{\text{Z, off-shell}}$$

$$\mu_{\text{on-shell}} = \frac{\sigma^{gg\to H\to ZZ^*}_{\text{on-shell}}}{\sigma^{gg\to H\to ZZ^*}_{\text{on-shell, SM}}} = \frac{k^2_{\text{g, on-shell}} \cdot k^2_{\text{Z, on-shell}}}{\Gamma_H/\Gamma_H^{SM}}$$

k_g and **k_Z** are the off(on)-shell coupling relative to the SM predictions associated to gg → H* production and H* → ZZ decay
they are assumed to be the same in the off- and on-shell process

$$\frac{\mu_{\text{off-shell}}}{\mu_{\text{on-shell}}} \sim \frac{\Gamma_H}{\Gamma_H^{SM}}$$

Higgs boson width measurement: constraints

PLB 786 (2018) 223-244 **ATLAS** 36 fb^{-1}

$H \to ZZ^* \to 4l / 2l2\nu$ $H \to ZZ \to 4l / 2l2\nu$

Strategy of 4l
- follows closely the H→4l analysis
  - on-shell: **m_{4l} [118,129] GeV**
  - off-shell: **m_{4l} [220,2000] GeV**
  - 3 categories: 4e, 2e2μ and 4μ

Strategy of 2l2v
- follows closely the search for ZZ→2l2v
  - off-shell: **m_{4l} [250,2000] GeV**
  - m_T^{ZZ} to discriminate S from B and to enhance sensitivity

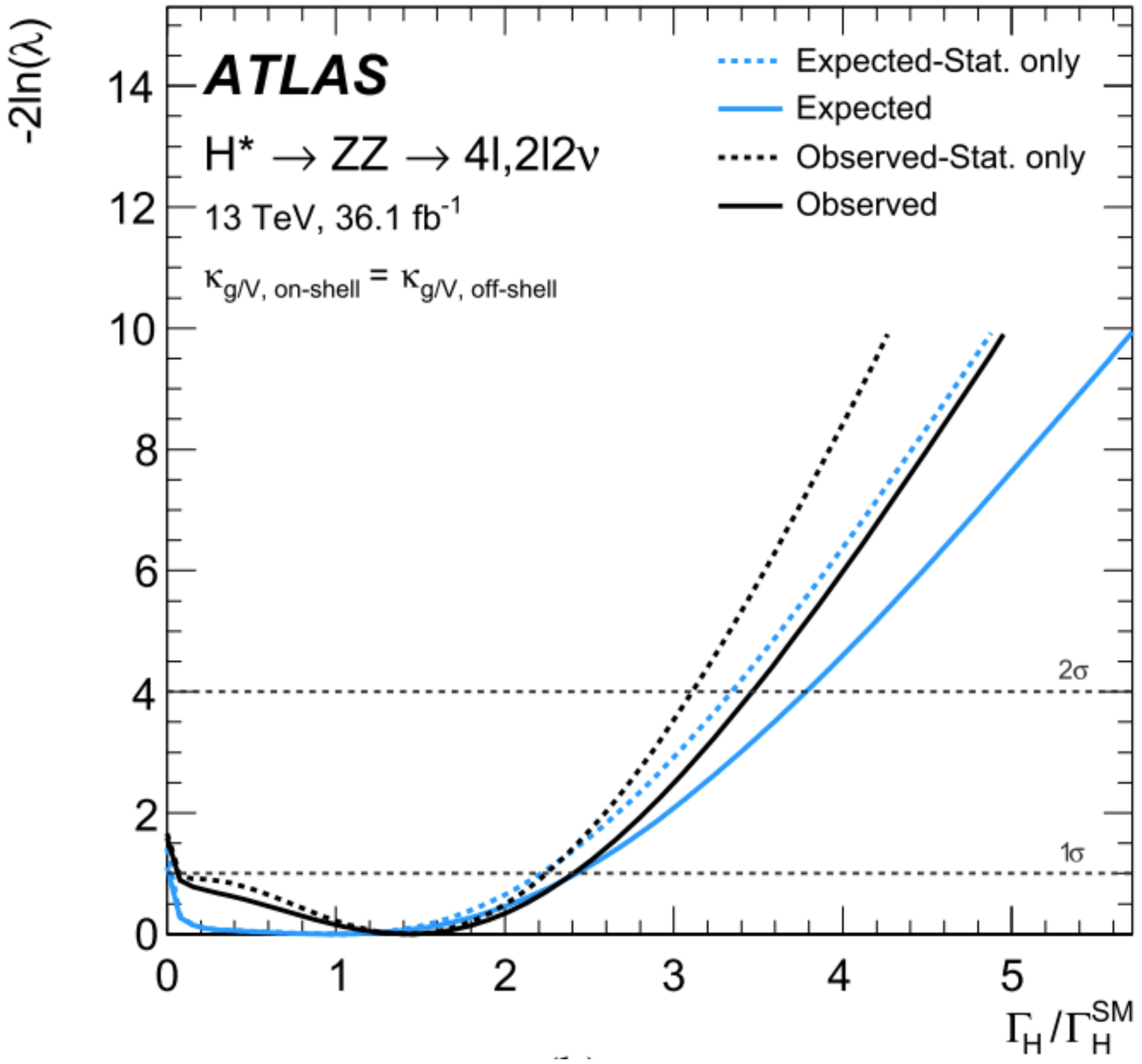

- ratio Γ_H/Γ_H^{SM} in plot

$\Gamma_H < 14.4$ (exp. 15.2) MeV

* generated from the likelihood distribution Λ with NPs fixed at the best fit value obtained on data and the POI fixed to SM hypothesis

24.8 fb^{-1}+80.2 fb^{-1} **CMS** JHEP 11 (2017) 047

$H \to ZZ^* \to 4l$ $H \to ZZ \to 4l$

Strategy
- follows closely the general H→4l selection and reconstruction
  - on-shell: **m_{4l} [105,140] GeV**
  - off-shell: **m_{4l} > 220 GeV**
  - 3 categories: 4e, 2e2μ and 4μ

- Run 1 + Run 2 combination

$\Gamma_H < 3.2$ (exp. 4.1) MeV

* generated from the likelihood distribution Λ with NPs fixed at the best fit value obtained on data and the POI fixed to SM hypothesis

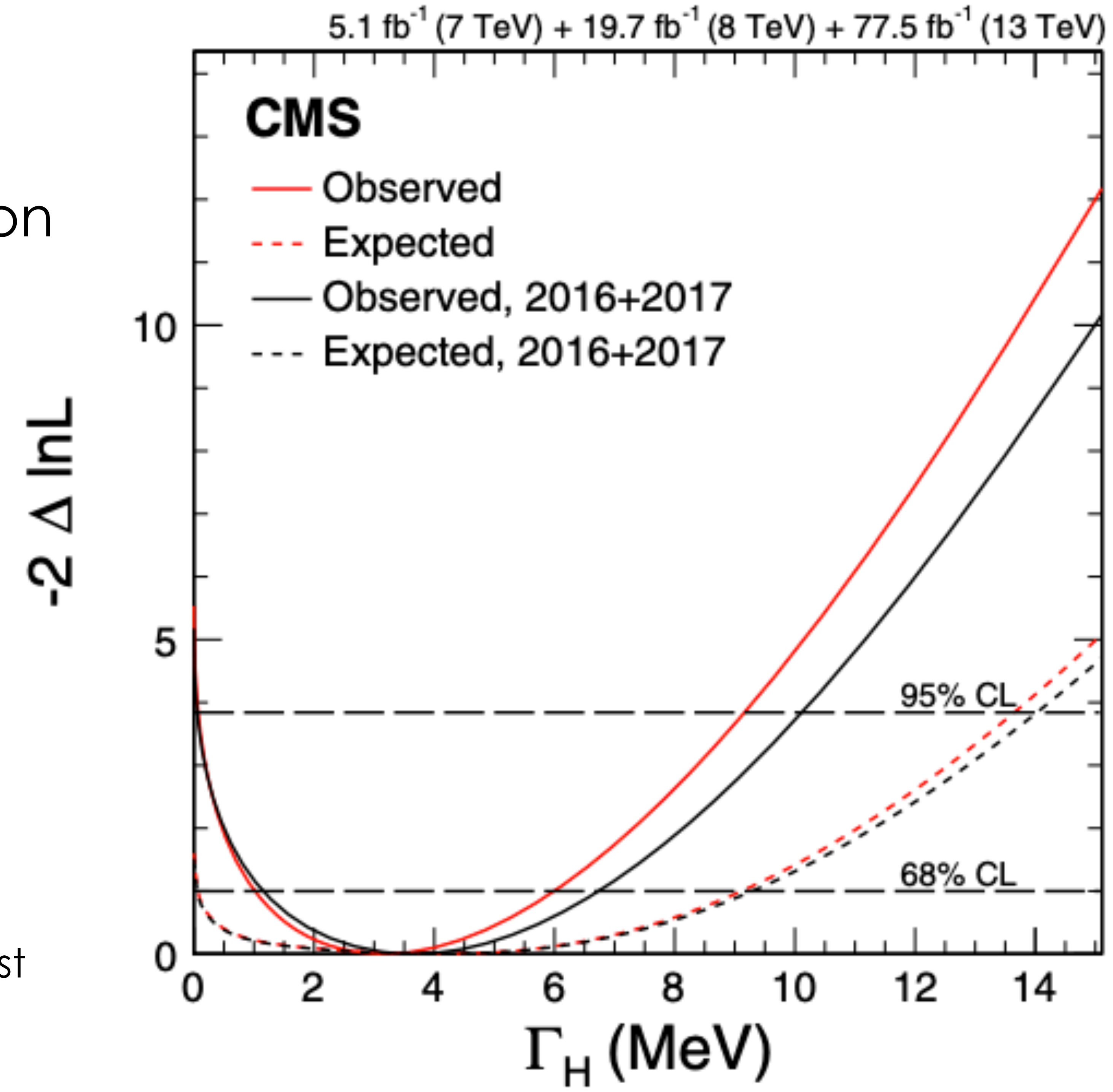

Search for $H \rightarrow \mu\mu$ decay mode

ATLAS-CONF-2019-028 **ATLAS** **139 fb^{-1} : 35.9 fb^{-1}** **CMS** PRL 122 (2019) 021801

Study of particular importance, because it extends the investigation to its couplings to fermions of the second generation

- expected BR to Higgs to muons is **2.17×10^{-4}**;
- Γ_H is several orders of magnitude smaller than the O(GeV) experimental di-muon mass resolution;
- signal would appear as a **narrow resonance over a smoothly falling mass spectrum** from the SM background processes, primarily Drell-Yan (DY), > 90%, and leptonic tt decays.

Strategy:

- events containing two opposite-charge muon candidates;
- 12 categories divided by **jet multiplicity and BDTs score** indicating probability of a specific Higgs production mode;
- **$110 < m_{\mu\mu} < 160$ GeV**.

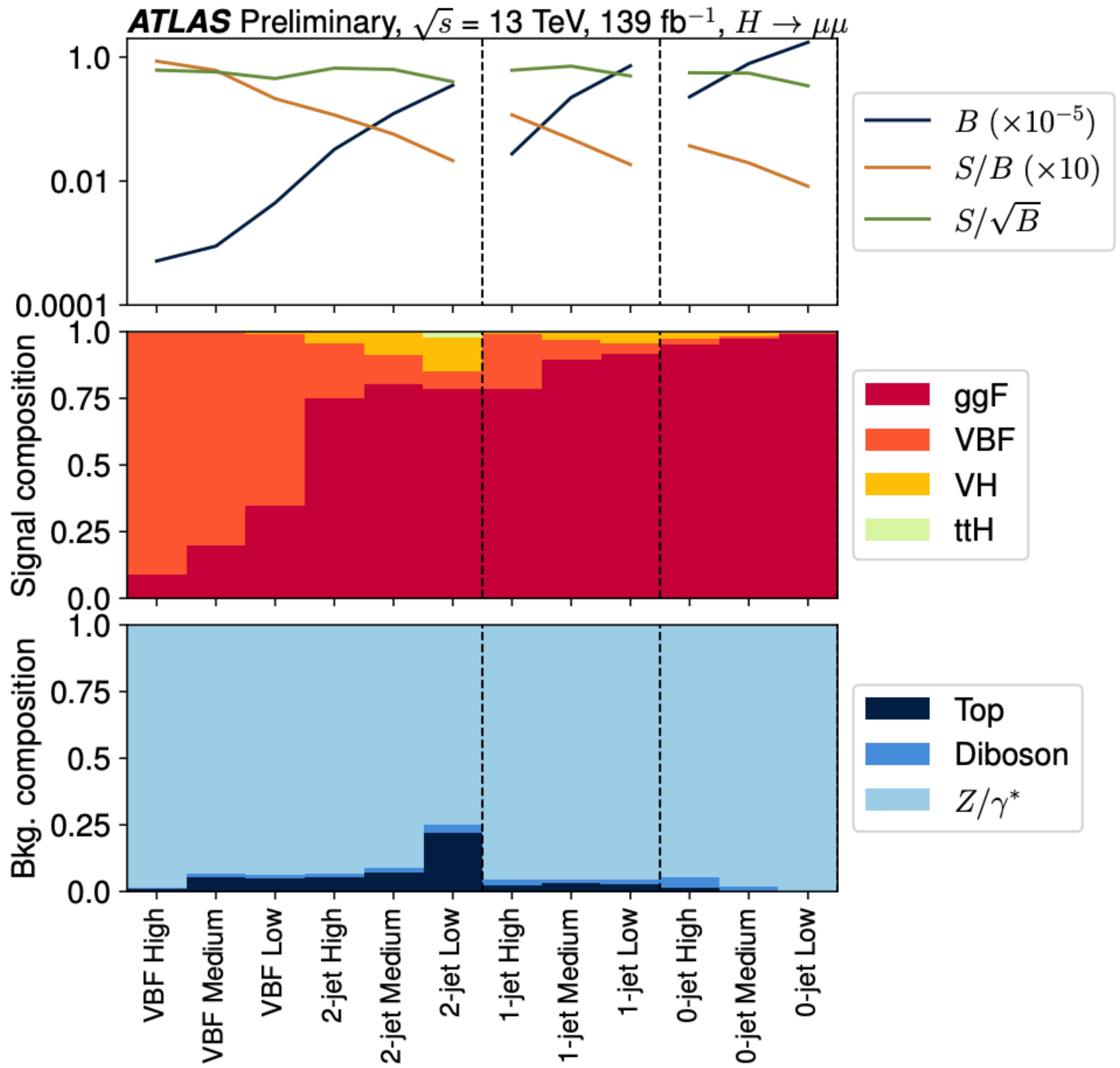

Strategy:

- events containing two opposite-charge muon candidates;
- 15 categories divided by **expected dimuon mass resolution and BDTs score** trained with uncorrelated variables with $m_{\mu\mu}$;
- **$110 < m_{\mu\mu} < 150$ GeV**.

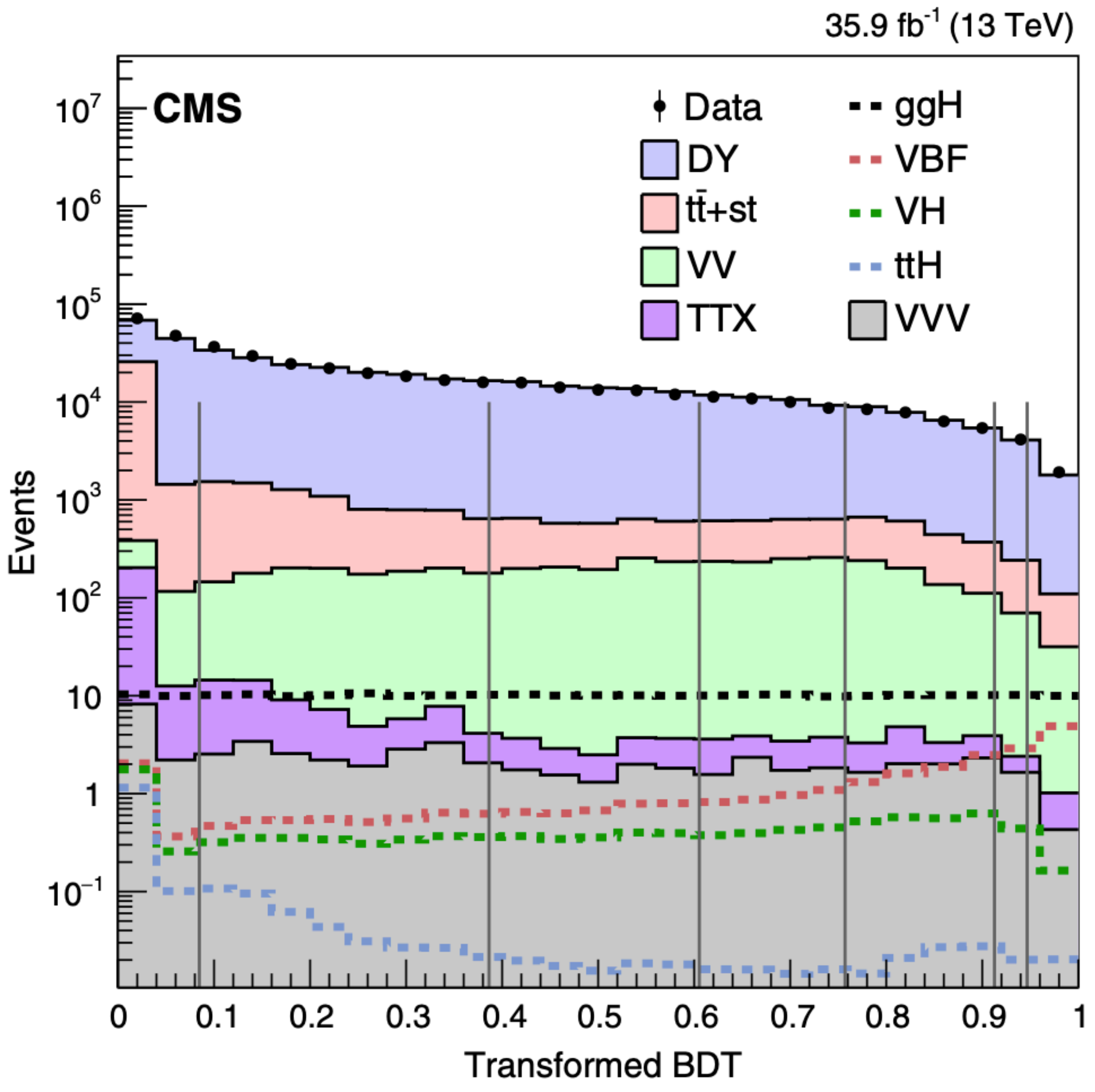

Search for H → μμ decay mode

ATLAS-CONF-2019-028 | ATLAS | 139 fb^{-1} : 35.9 fb^{-1} | CMS | PRL 122 (2019) 021801

Systematic uncertainties treatment

- **S/B ~ 0.2% in $m_{\mu\mu}$ = 120-130 GeV** → background determination is of paramount importance;
- **analytical function** to describe with high accuracy the main background;
- signal and background modelling are included in the uncertainties: accounting for possible mismodeling in the signal/bkg shape or rate;
- experimental systematic uncertainties dominated in each category by **jet energy scale and resolution and muon momentum resolution**.

Results:

- **improvement of about 50%** in expected sensitivity compared with the previous ATLAS result;
- half of this improvement comes from the **increased integrated luminosity** and half from **refinements in the analysis techniques**.

$$\mu = 0.5 \pm 0.7\ (\text{stat})\ {}^{+0.2}_{-0.1}\ (\text{syst})$$

$$\text{obs } 0.8\sigma\ (\text{exp } 1.5\sigma)$$

$$BR < 3.8 \cdot 10^{-4}$$

uncertainty dominated by the statistical error

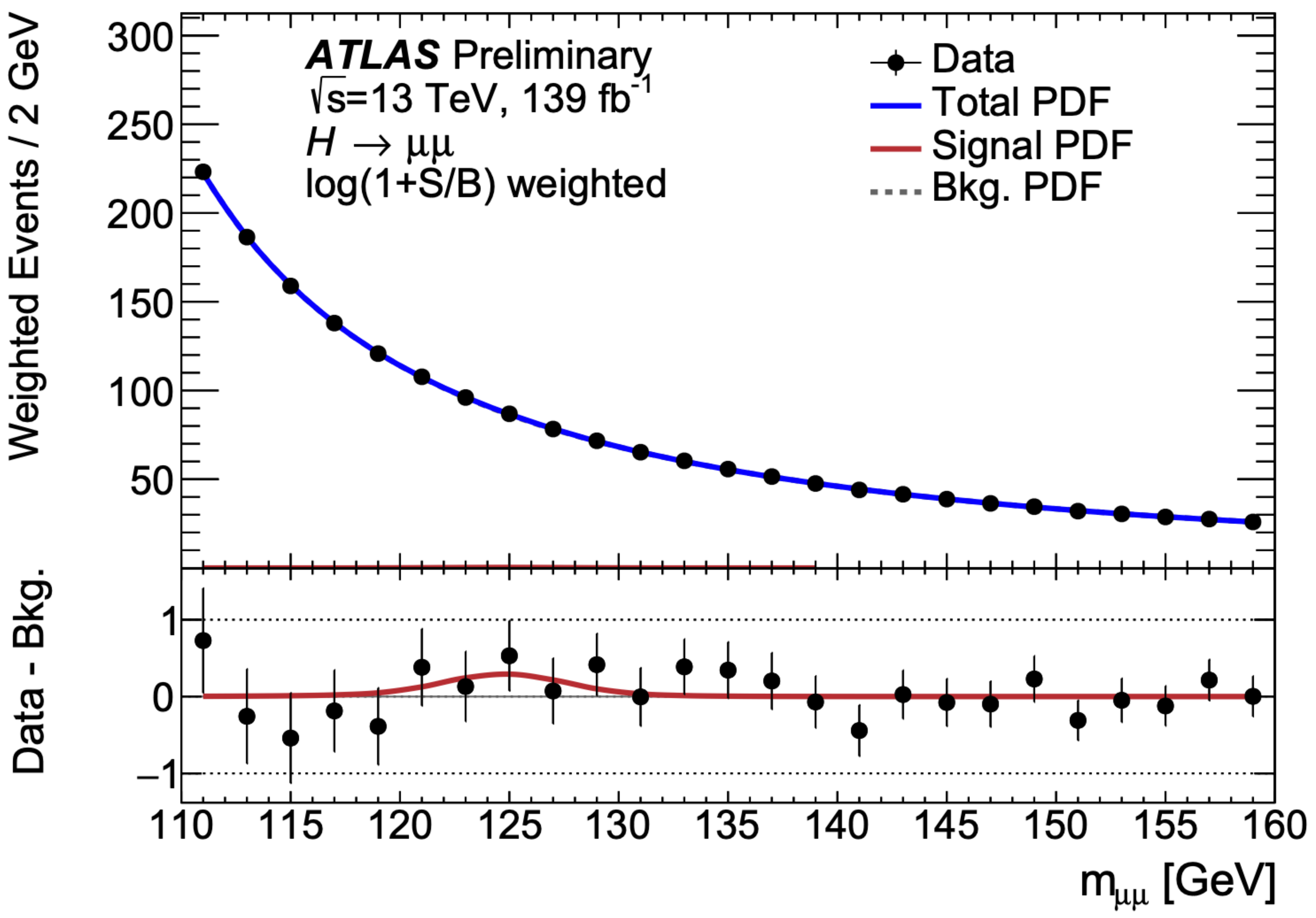

Results:

- **improvement of about 50%** in expected sensitivity compared with the previous CMS result;
- **combination with Run 1** datasets helps the improvement.

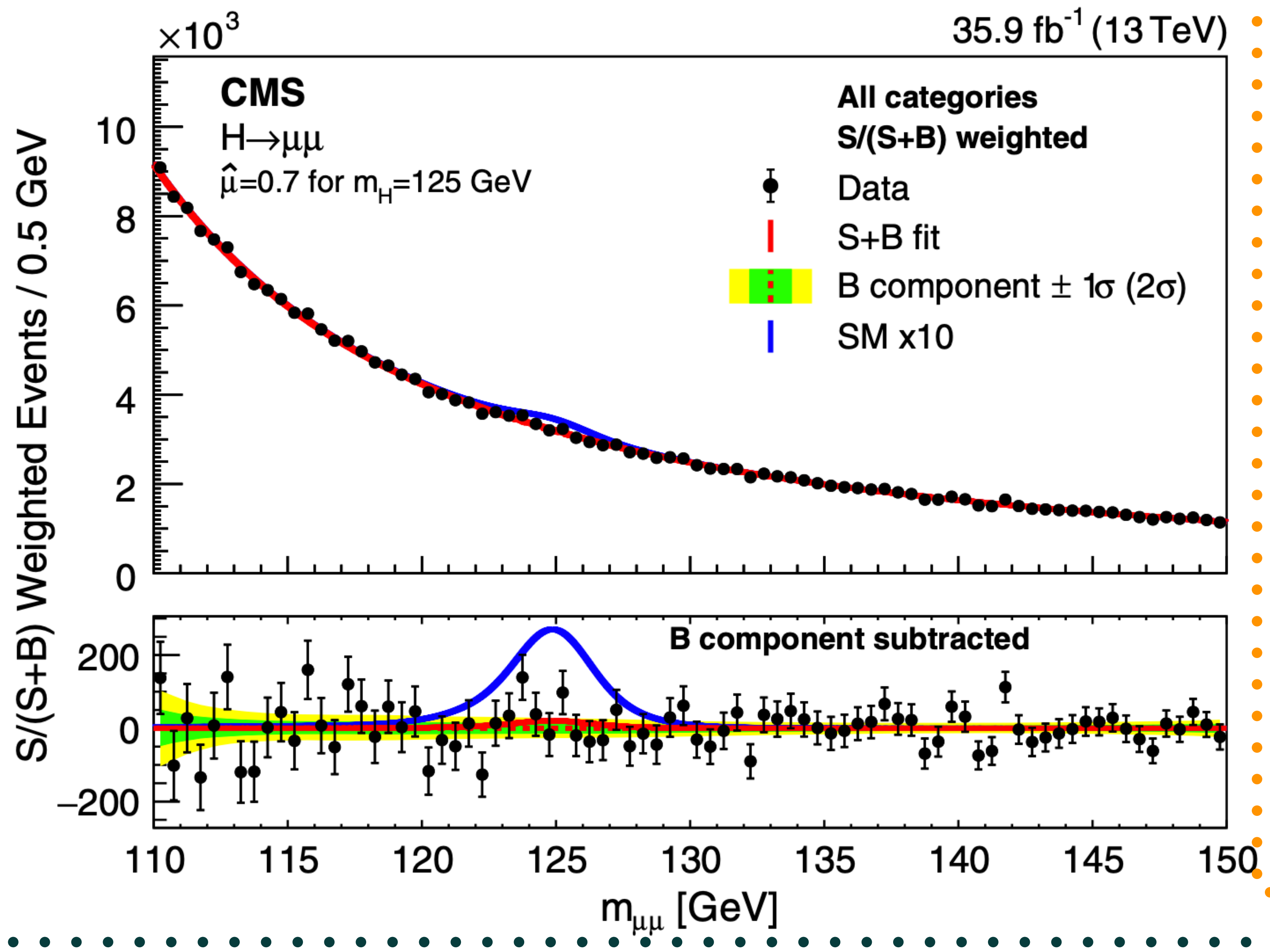

+ Run 1

$$\mu = 1.0 \pm 1.0\ (\text{stat})\ {}^{+0.1}_{-0.1}\ (\text{syst})$$

$$\text{obs } 0.9\sigma\ (\text{exp } 1.0\sigma)$$

$$BR < 6.4 \cdot 10^{-4}$$

uncertainty dominated by the statistical error

Higgs self-coupling constraints

ATLAS only ATL-PHYS-PUB-2019-009

$$H \to \gamma\gamma, ZZ^*, WW^*, \tau\tau, b\bar{b}, \mu\mu$$

up to 79.8 fb^{-1}

Properties of the Higgs scalar potential (i.e. Higgs self-coupling), still largely unconstrained

- **Higgs trilinear self-coupling contributions λ_{HHH}** need to be taken into account for the calculation of the next-to-leading (NLO) EW corrections;
- an indirect constraint on λ_{HHH} by comparing precise measurements of **single Higgs production** yields and the **SM predictions corrected for the λ_{HHH}-dependent NLO EW effects**.

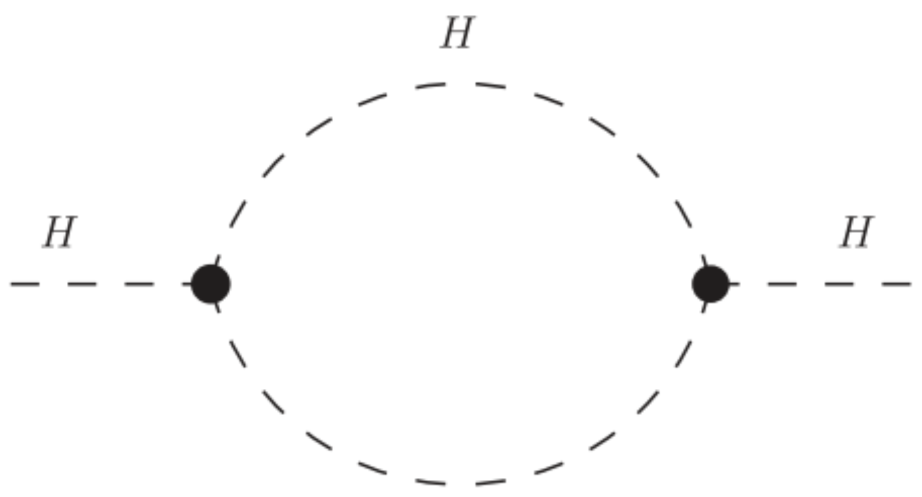

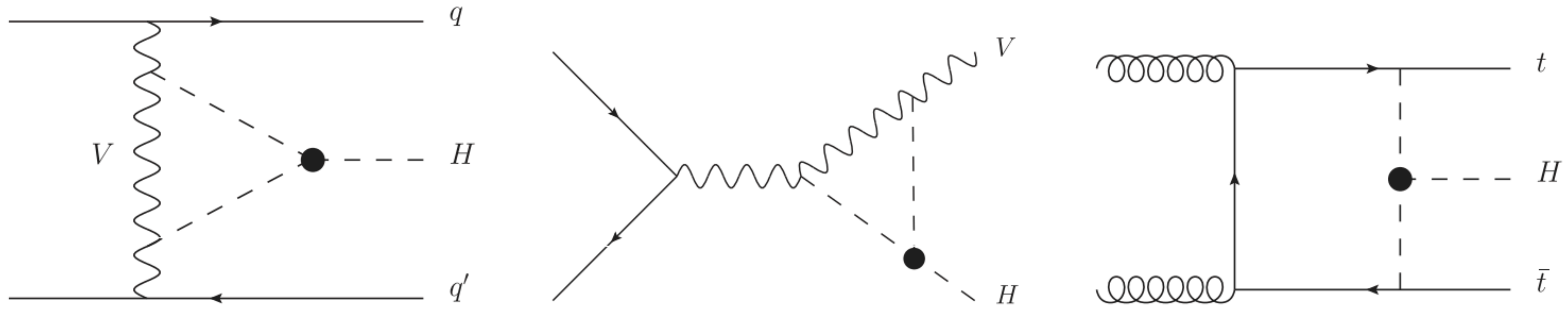

Strategy:

- overall **61 event categories among the analyses**;
- differential xsec measurements in VBF and VH processes, just one bin in ttH;
- varied Higgs trilinear coupling, **changes in κ_λ** affect not only the inclusive rates of Higgs boson production and decay processes, but also their kinematics;
- accounting for effect due to the **variation of the trilinear coupling λ_{HHH}**: both production cross section and BRs.

$$\mu_i(\kappa_\lambda, \kappa_i) = \frac{\sigma^{BSM}}{\sigma^{SM}}$$

$$\mu_f(\kappa_\lambda, \kappa_f) = \frac{BR_f^{BSM}}{BR_f^{SM}}$$

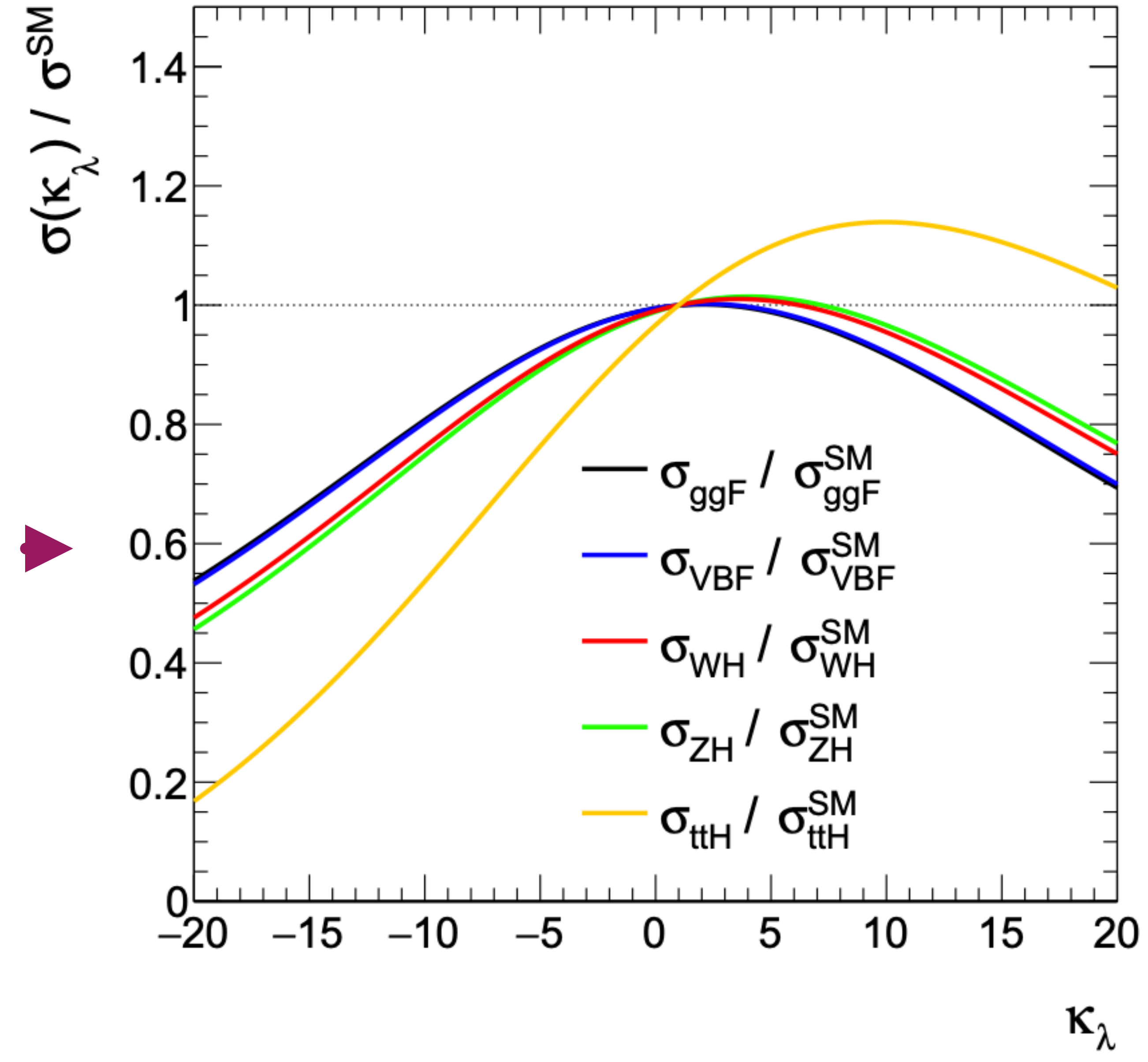

Higgs self-coupling constraints

ATLAS only ATL-PHYS-PUB-2019-009

$H \to \gamma\gamma, ZZ^*, WW^*, \tau\tau, b\bar{b}, \mu\mu$

up to 79.8 fb^{-1}

Strategy:

- likelihood fit is performed **to constrain the value of the Higgs boson self-coupling κ_λ**;
- leaving untouched all other Higgs boson couplings ($\kappa_V = \kappa_F = 1$);
- global fit to $\kappa_\lambda = \lambda_{HHH}/\lambda_{HHH}^{SM}$ in the range $-20 < \kappa_\lambda < 20$;
- **only two coupling modifiers κ_F and κ_V are considered**.

* generated from the likelihood distribution Λ with NPs fixed at the best fit value obtained on data and the POI fixed to SM hypothesis

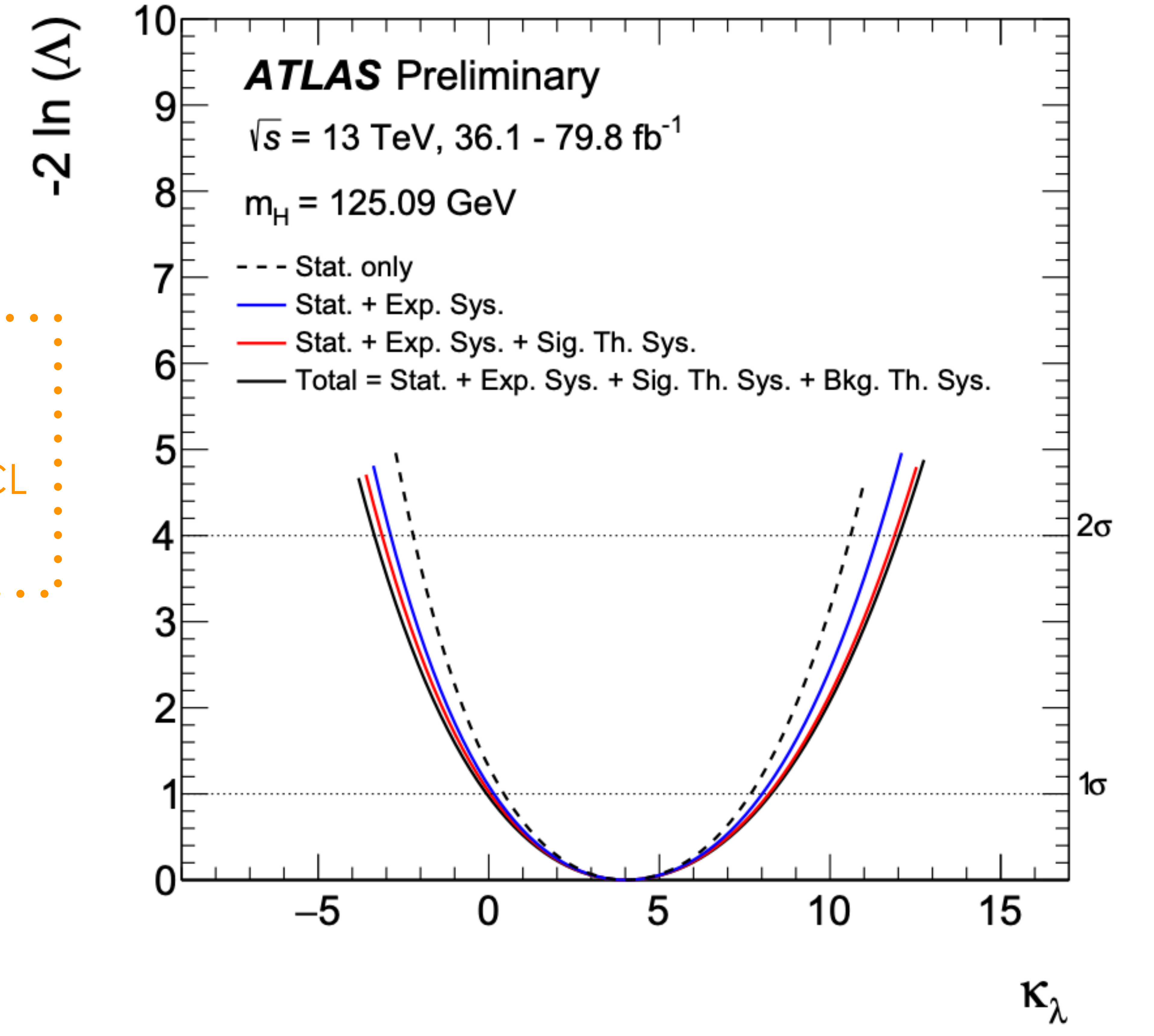

Results:

- differential information currently provided by the STXS regions in the VBF, WH and ZH production modes does not help to improve the sensitivity to κ_λ significantly;
- a **dedicated optimisation of the kinematic binning**, including the most sensitive ggF and ttH production modes, still needs to be fully theoretically and experimentally explored and **might improve the sensitivity in the future**.

$$\kappa_\lambda = 4.0^{+4.3}_{-4.1}$$

excluded values at 95% CL

$$-3.2 < \kappa_\lambda < 11.9$$

Higgs self-coupling constraints

ATLAS only ATL-PHYS-PUB-2019-009

$H \to \gamma\gamma, ZZ^*, WW^*, \tau\tau, b\bar{b}, \mu\mu$

up to 79.8 fb^{-1}

Two additional fit configurations are considered in this note, in which a simultaneous fit is performed to κ_λ and κ_F, or to κ_λ and κ_V

- remaining coupling modifier that is not included in the fit, κ_V in the first case and κ_F in the second case, is kept fixed to the SM prediction;
- **target BSM scenarios** where new physics could affect only the Yukawa type terms ($\kappa_V = 1$) of the SM or only the couplings to vector bosons ($\kappa_F = 1$), in addition to the Higgs boson self-coupling (κ_λ).

Results:

- As expected, **including additional degrees of freedom to the fit reduces the constraining power of the measurement**;
- sensitivity to κ_λ is not much degraded when determining κ_F at the same time, while it is degraded by 50% (on the expected lower 95% C.L. exclusion limit) when determining simultaneously κ_V and κ_λ.

constraints become significantly weaker in new physics scenarios where simultaneous modifications to the single Higgs boson couplings are allowed

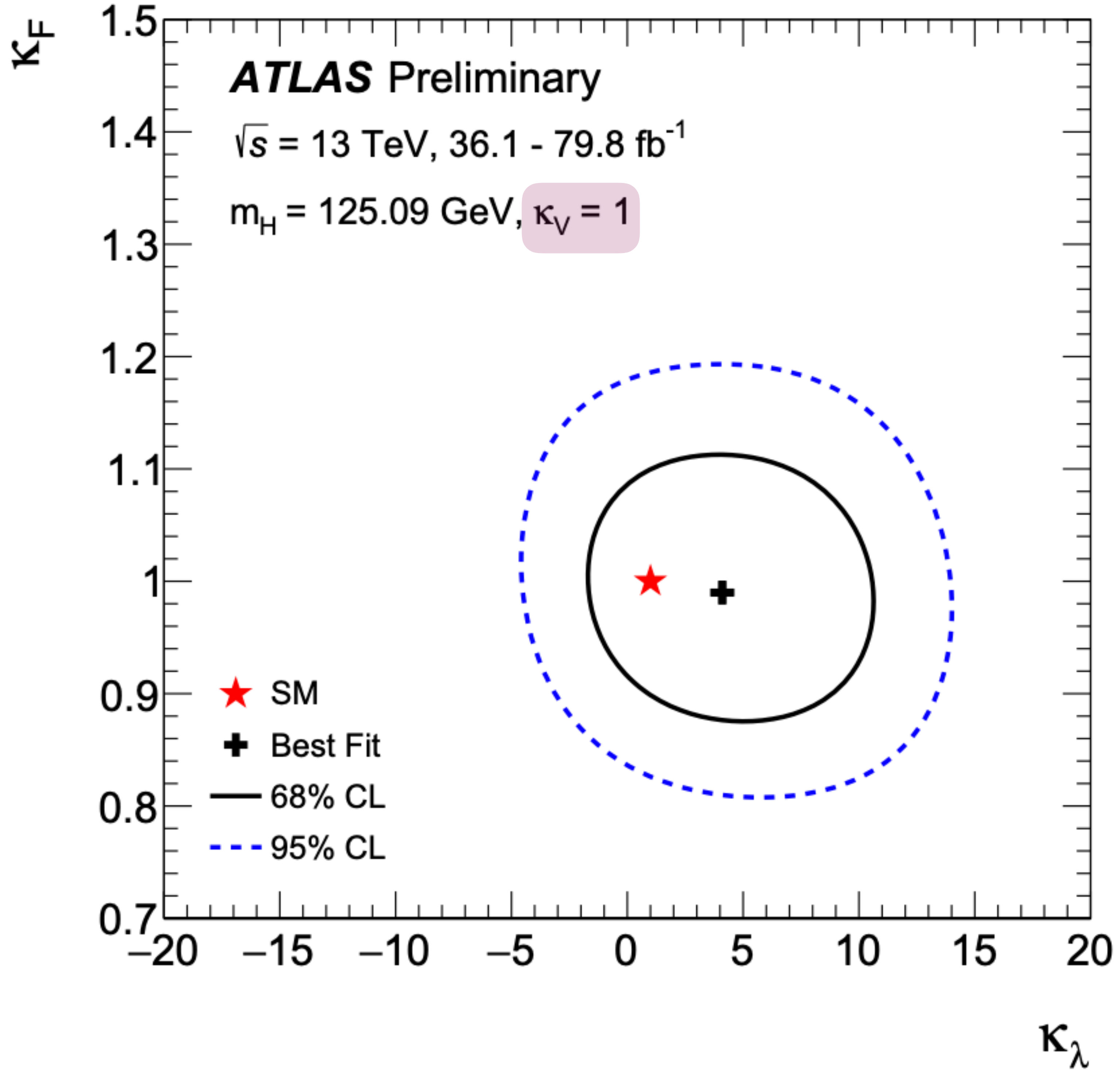

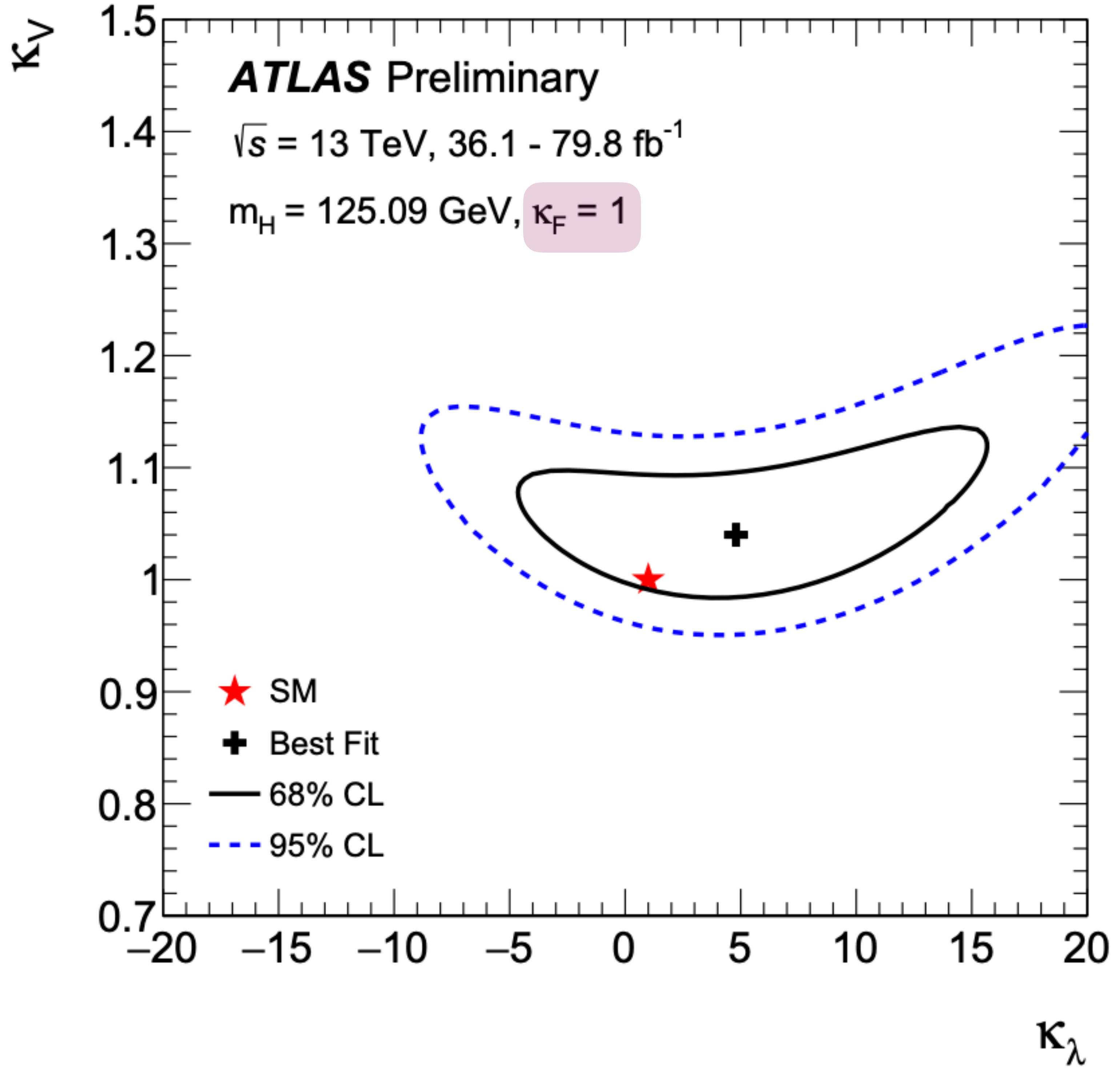

Supporting material

LHC / HL-LHC plan

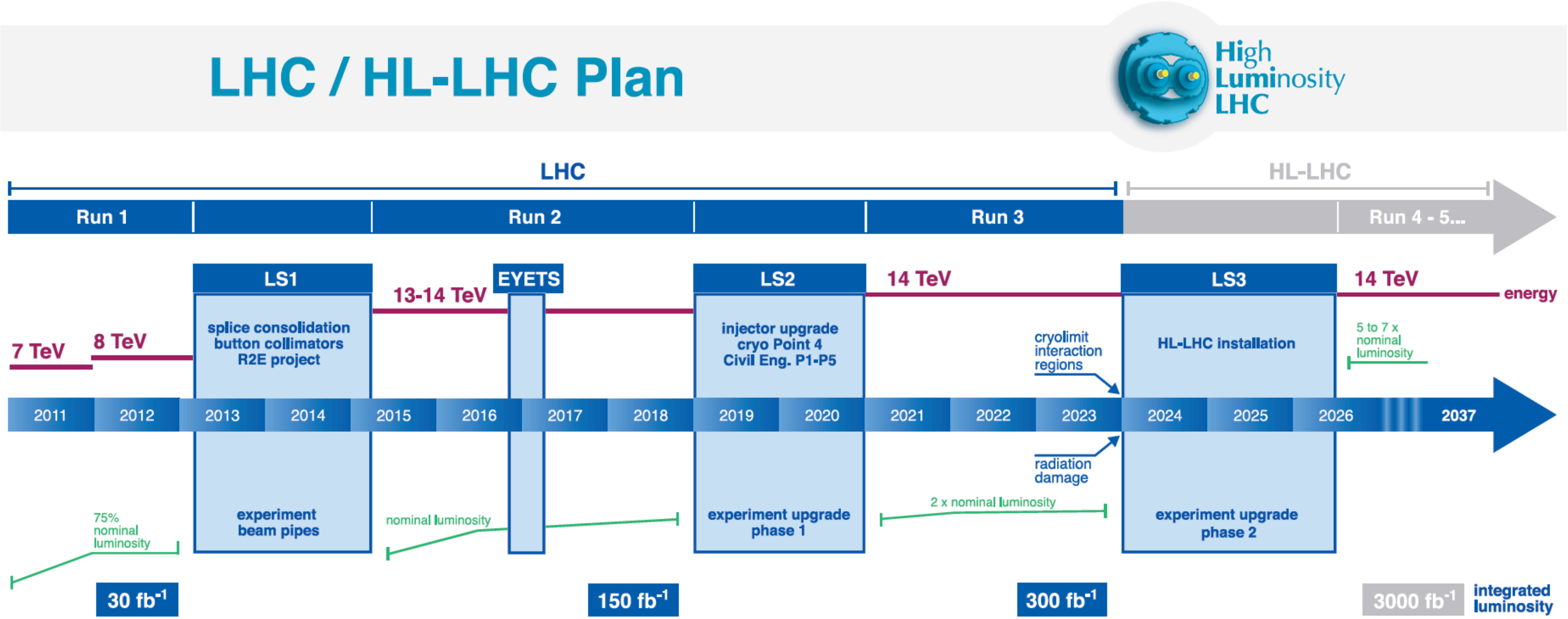

Higgs boson mass measurement: new results

PLB 784 (2018) 345

ATLAS

36 fb^{-1}

$H \to ZZ^* \to 4l$

$H \to \gamma\gamma$

m_H = 124.79 ± 0.37 GeV

m_H = 124.93 ± 0.40 GeV

m_H = 124.86 ± 0.27 (± 0.18) GeV

*no Run 1 combination for this result, the full combination is shown in the main body

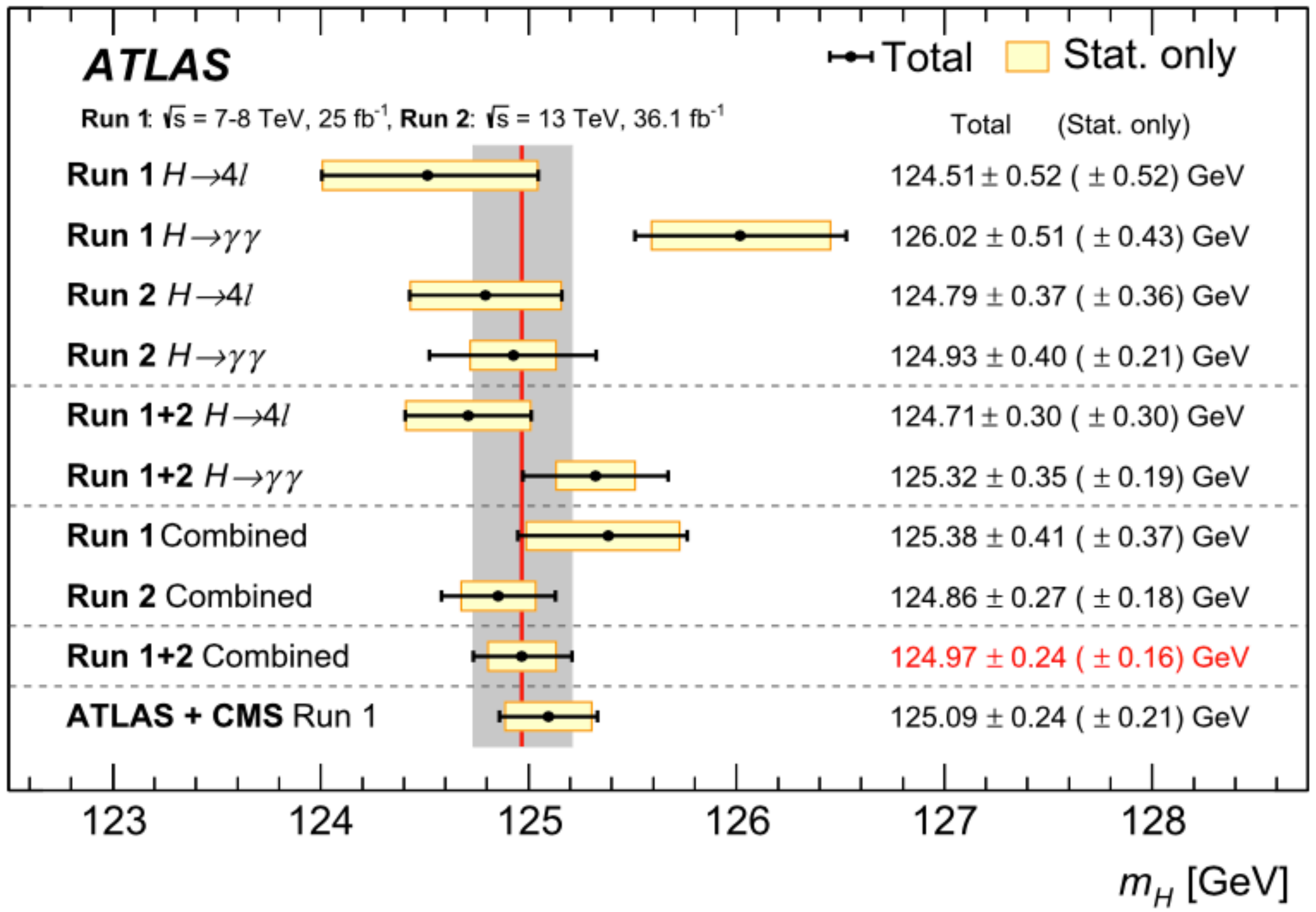

35.9 fb^{-1}

CMS

JHEP 11 (2017) 047

$H \to ZZ^* \to 4l$

Strategy:

- more complex wrt previous H→4l analysis:
  - 7 categories based on jet multiplicity, leptons, kinematics discriminants (sensitive to differente production modes and jets production), etc
  - definitions of the categories were chosen to achieve high signal purity whilst maintaining high efficiency for each of the main Higgs boson production mechanisms.

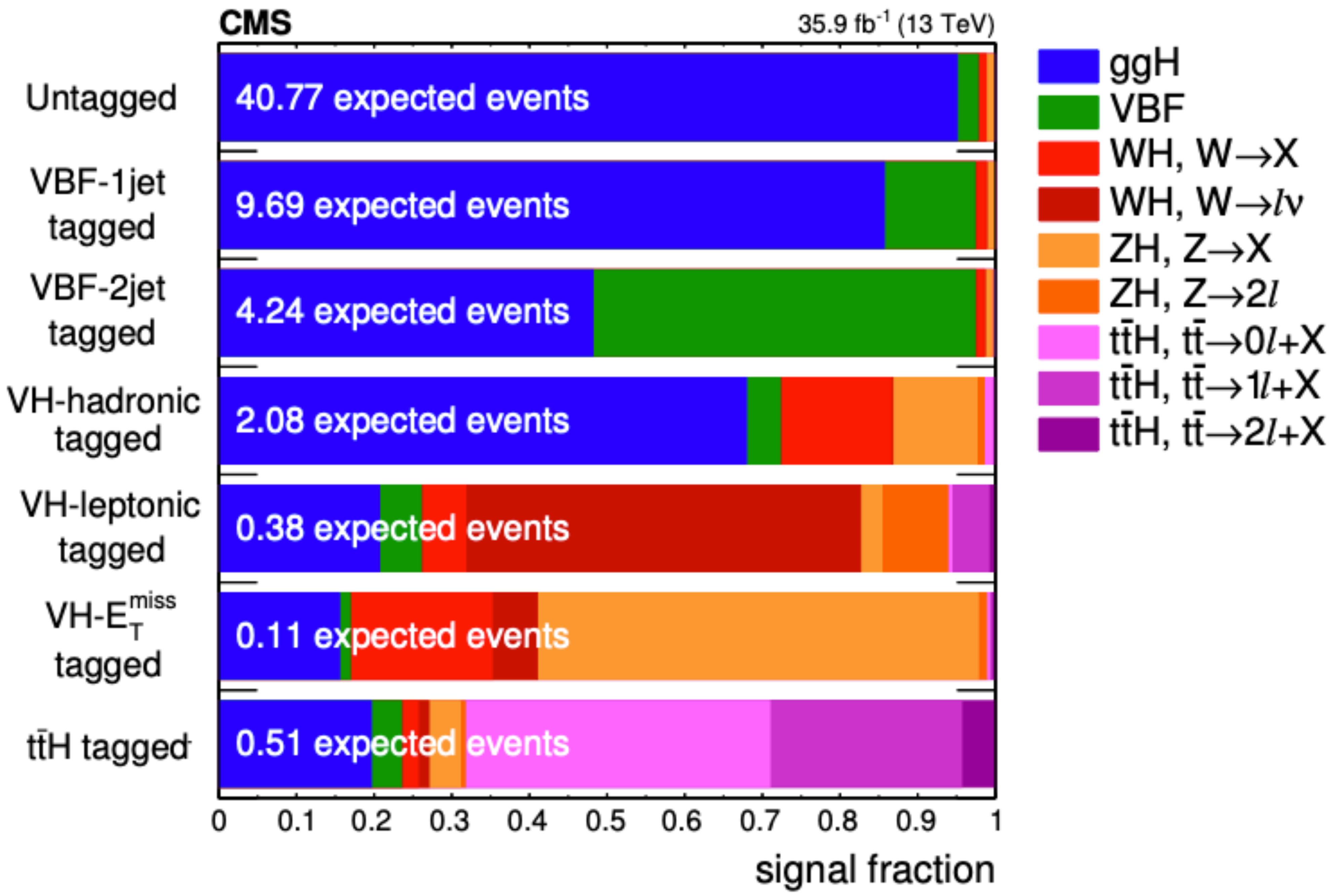

Higgs boson mass measurement: new results

PLB 784 (2018) 345

ATLAS

36 fb^{-1}

$H \rightarrow ZZ^* \rightarrow 4l$

m_H = 124.79 ± 0.37 GeV

$H \rightarrow \gamma\gamma$

m_H = 124.93 ± 0.40 GeV

m_H = 124.86 ± 0.27 (± 0.18) GeV

*no Run 1 combination for this result, the full combination is shown in the main body

Table 1
Main sources of systematic uncertainty in the Higgs boson mass m_H measured with the 4ℓ and $\gamma\gamma$ final states using Run 1 and Run 2 data. The sum in quadrature of the individual contributions is not expected to reproduce the total systematic uncertainty due to the different methodologies employed to derive them.

Source	Systematic uncertainty in m_H [MeV]
EM calorimeter response linearity	60
Non-ID material	55
EM calorimeter layer intercalibration	55
$Z \rightarrow ee$ calibration	45
ID material	45
Lateral shower shape	40
Muon momentum scale	20
Conversion reconstruction	20
$H \rightarrow \gamma\gamma$ background modelling	20
$H \rightarrow \gamma\gamma$ vertex reconstruction	15
e/γ energy resolution	15
All other systematic uncertainties	10

CMS

35.9 fb^{-1}

JHEP 11 (2017) 047

$H \rightarrow ZZ^* \rightarrow 4l$

Main systematic uncertainties:
- lepton energy scale
- 4l mass resolution (20%)
- lepton identification and reconstruction efficiency (from 2.5 to 9%)
- integrated luminosity (2.5%)

Higgs boson cross-section measurement: inclusive

PRD 101 (2020) 012002 — **ATLAS**

	$H\to\gamma\gamma$	$H\to ZZ^*$	$H\to WW^*$	$H\to\tau\tau$	$H\to b\bar{b}$
$t\bar{t}H$	$t\bar{t}H$ leptonic (3 categories) $t\bar{t}H$ hadronic (4 categories)	$t\bar{t}H$ multilepton 1 ℓ + 2 τ_{had} $t\bar{t}H$ multilepton 2 opposite-sign ℓ + 1 τ_{had} $t\bar{t}H$ multilepton 2 same-sign ℓ (categories for 0 or 1 τ_{had}) $t\bar{t}H$ multilepton 3 ℓ (categories for 0 or 1 τ_{had}) $t\bar{t}H$ multilepton 4 ℓ (except $H\to ZZ^*\to 4\ell$) $t\bar{t}H$ leptonic, $H\to ZZ^*\to 4\ell$ $t\bar{t}H$ hadronic, $H\to ZZ^*\to 4\ell$			$t\bar{t}H$ 1 ℓ, boosted $t\bar{t}H$ 1 ℓ, resolved (11 categories) $t\bar{t}H$ 2 ℓ (7 categories)
VH	VH 2 ℓ VH 1 ℓ, $p_T^{\ell+E_T^{miss}} \geq 150$ GeV VH 1 ℓ, $p_T^{\ell+E_T^{miss}} < 150$ GeV VH E_T^{miss}, $E_T^{miss} \geq 150$ GeV VH E_T^{miss}, $E_T^{miss} < 150$ GeV VH+VBF $p_T^{j1} \geq 200$ GeV VH hadronic (2 categories)	VH leptonic 0-jet, $p_T^{4\ell} \geq 100$ GeV 2-jet, $m_{jj} < 120$ GeV			2 ℓ, $75 \leq p_T^V < 150$ GeV, $N_{jets} = 2$ 2 ℓ, $75 \leq p_T^V < 150$ GeV, $N_{jets} \geq 3$ 2 ℓ, $p_T^V \geq 150$ GeV, $N_{jets} = 2$ 2 ℓ, $p_T^V \geq 150$ GeV, $N_{jets} \geq 3$ 1 ℓ $p_T^V \geq 150$ GeV, $N_{jets} = 2$ 1 ℓ $p_T^V \geq 150$ GeV, $N_{jets} = 3$ 0 ℓ, $p_T^V \geq 150$ GeV, $N_{jets} = 2$ 0 ℓ, $p_T^V \geq 150$ GeV, $N_{jets} = 3$
VBF	VBF, $p_T^{\gamma\gamma jj} \geq 25$ GeV (2 categories) VBF, $p_T^{\gamma\gamma jj} < 25$ GeV (2 categories)	2-jet VBF, $p_T^{j1} \geq 200$ GeV 2-jet VBF, $p_T^{j1} < 200$ GeV	2-jet VBF	VBF $p_T^{\tau\tau} > 140$ GeV ($\tau_{had}\tau_{had}$ only) VBF high-m_{jj} VBF low-m_{jj}	VBF, two central jets VBF, four central jets VBF+γ
ggF	2-jet, $p_T^{\gamma\gamma} \geq 200$ GeV 2-jet, 120 GeV$\leq p_T^{\gamma\gamma} <$200 GeV 2-jet, 60 GeV$\leq p_T^{\gamma\gamma} <$120 GeV 2-jet, $p_T^{\gamma\gamma} < 60$ GeV 1-jet, $p_T^{\gamma\gamma} \geq 200$ GeV 1-jet, 120 GeV$\leq p_T^{\gamma\gamma} <$200 GeV 1-jet, 60 GeV$\leq p_T^{\gamma\gamma} <$120 GeV 1-jet, $p_T^{\gamma\gamma} < 60$ GeV 0-jet (2 categories)	1-jet, $p_T^{4\ell} \geq 120$ GeV 1-jet, 60 GeV$\leq p_T^{4\ell} <$120 GeV 1-jet, $p_T^{4\ell} < 60$ GeV 0-jet, $p_T^{4\ell} < 100$ GeV	1-jet, $m_{\ell\ell} < 30$ GeV, $p_T^{\ell_2} < 20$ GeV 1-jet, $m_{\ell\ell} < 30$ GeV, $p_T^{\ell_2} \geq 20$ GeV 1-jet, $m_{\ell\ell} \geq 30$ GeV, $p_T^{\ell_2} < 20$ GeV 1-jet, $m_{\ell\ell} \geq 30$ GeV, $p_T^{\ell_2} \geq 20$ GeV 0-jet, $m_{\ell\ell} < 30$ GeV, $p_T^{\ell_2} < 20$ GeV 0-jet, $m_{\ell\ell} < 30$ GeV, $p_T^{\ell_2} \geq 20$ GeV 0-jet, $m_{\ell\ell} \geq 30$ GeV, $p_T^{\ell_2} < 20$ GeV 0-jet, $m_{\ell\ell} \geq 30$ GeV, $p_T^{\ell_2} \geq 20$ GeV	Boosted, $p_T^{\tau\tau} > 140$ GeV Boosted, $p_T^{\tau\tau} \leq 140$ GeV	

CMS — **EPJC 79 (2019) 421**

Decay tags	Production tags	Number of categories	Expected signal fractions	Mass resolution
$H\to\gamma\gamma$, Sect. 3.1				
$\gamma\gamma$	Untagged	4	74–91% ggH	≈1–2%
	VBF	3	51–80% VBF	
	VH hadronic	1	25% WH, 15% ZH	
	WH leptonic	2	64–83% WH	
	ZH leptonic	1	98% ZH	
	VH p_T^{miss}	1	59% VH	
	ttH	2	80–89% ttH, ≈8% tH	
$H\to ZZ^{(*)}\to 4\ell$, Sect. 3.2				
4μ, $2e2\mu/2\mu 2e$, 4e	Untagged	3	≈95% ggH	≈1–2%
	VBF 1, 2-jet	6	≈11–47% VBF	
	VH hadronic	3	≈13% WH, ≈10% ZH	
	VH leptonic	3	≈46% WH	
	VH p_T^{miss}	3	≈56% ZH	
	ttH	3	≈71% ttH	
$H\to WW^{(*)}\to \ell\nu\ell\nu$, Sect. 3.3				
$e\mu/\mu e$	ggH 0, 1, 2-jet	17	≈55–92% ggH, up to ≈15% $H\to\tau\tau$	≈20%
	VBF 2-jet	2	≈47% VBF, up to ≈25% $H\to\tau\tau$	
ee+$\mu\mu$	ggH 0, 1-jet	6	≈84–94% ggH	
$e\mu$+jj	VH 2-jet	1	22% VH, 21% $H\to\tau\tau$	
3ℓ	WH leptonic	2	≈80% WH, up to 19% $H\to\tau\tau$	
4ℓ	ZH leptonic	2	85–90% ZH, up to 14% $H\to\tau\tau$	
$H\to\tau\tau$, Sect. 3.4				
$e\mu$, $e\tau_h$, $\mu\tau_h$, $\tau_h\tau_h$	0-jet	4	≈70–98% ggH, 29% $H\to WW$ in $e\mu$	≈10–20%
	VBF	4	≈35–60% VBF, 42% $H\to WW$ in $e\mu$	
	Boosted	4	≈48–83% ggH, 43% $H\to WW$ in $e\mu$	
VH production with $H\to$ bb, Sect. 3.5				
$Z(\nu\nu)H(bb)$	ZH leptonic	1	≈100% VH, 85% ZH	≈10%
$W(\ell\nu)H(bb)$	WH leptonic	2	≈100% VH, ≈97% WH	
$Z(\ell\ell)H(bb)$	Low-p_T(V) ZH leptonic	2	≈100% ZH, of which ≈20% ggZH	
	High-p_T(V) ZH leptonic	2	≈100% ZH, of which ≈36% ggZH	
Boosted H Production with $H\to$ bb, Sect. 3.6				
bb	p_T(H) bins	6	≈72–79% ggH	≈10%
ttH production with $H\to$ leptons, Sect. 3.7.1				
2ℓss	ttH	10	$WW/\tau\tau \approx 4.5$, ≈5% tH	
3ℓ		4	$WW:\tau\tau:ZZ \approx 15:4:1$, ≈5% tH	
4ℓ		1	$WW:\tau\tau:ZZ \approx 6:1:1$, ≈3% tH	
$1\ell+2\tau_h$		1	96% ttH with $H\to\tau\tau$, ≈6% tH	
2ℓss$+1\tau_h$		2	$\tau\tau:WW \approx 5:4$, ≈5% tH	
$3\ell+1\tau_h$		1	$\tau\tau:WW:ZZ \approx 11:7:1$, ≈3% tH	
ttH production with $H\to$ bb, Sect. 3.7.2				
bb	$t\bar{t}\to$ jets	6	≈83–97% ttH with $H\to$ bb	

Higgs boson cross-section measurement: inclusive

PRD 101 (2020) 012002 **ATLAS**

The number of signal events in each analysis category k is expressed as

$$n_k^{\text{signal}} = \mathcal{L}_k \sum_i \sum_f (\sigma \times B)_{if} (A \times \epsilon)_{if,k} \quad (1)$$

where the sum runs over production modes i (i = ggF, VBF, WH, ZH, $t\bar{t}H, \ldots$) and decay final states f ($f = \gamma\gamma, ZZ^*, WW^*, \tau\tau, b\bar{b}, \mu\mu$), $\mathcal{L}_k$ is the integrated luminosity of the dataset used in category k, and $(A \times \epsilon)_{if,k}$ is the acceptance times efficiency factor in category k for production mode i and final state f. The cross section times branching fraction $(\sigma \times B)_{if}$ for each relevant pair (i, f) are the parameters of interest of the model. The measurements presented in this paper are obtained from fits in which these

Uncertainty source	$\Delta\mu/\mu$ [%]
Statistical uncertainty	4.4
Systematic uncertainties	6.2
Theory uncertainties	4.8
Signal	4.2
Background	2.6
Experimental uncertainties (excl. MC stat.)	4.1
Luminosity	2.0
Background modeling	1.6
Jets, E_T^{miss}	1.4
Flavor tagging	1.1
Electrons, photons	2.2
Muons	0.2
τ-lepton	0.4
Other	1.6
MC statistical uncertainty	1.7
Total uncertainty	7.6

CMS EPJC 79 (2019) 421

Decay tags	Production tags	Number of categories	Expected signal fractions	Mass resolution
	$t\bar{t} \to 1\ell$+jets	18	≈65–95% ttH with H → bb, up to 20% H → WW	
	$t\bar{t} \to 2\ell$+jets	3	≈84–96% ttH with H → bb	
Search for H → $\mu\mu$, Sect. 3.8				
$\mu\mu$	S/B bins	15	56–96% ggH, 1–42% VBF	≈1–2%
Search for invisible H decays, Sect. 3.9				
Invisible	VBF	1	52% VBF, 48% ggH	
	ggH + ≥ 1 jet	1	80% ggH, 9% VBF	
	VH hadronic	1	54% VH, 39% ggH	
	ZH leptonic	1	≈100% ZH, of which 21% ggZH	

Higgs boson cross-section measurement: inclusive

PRD 101 (2020) 012002

ATLAS

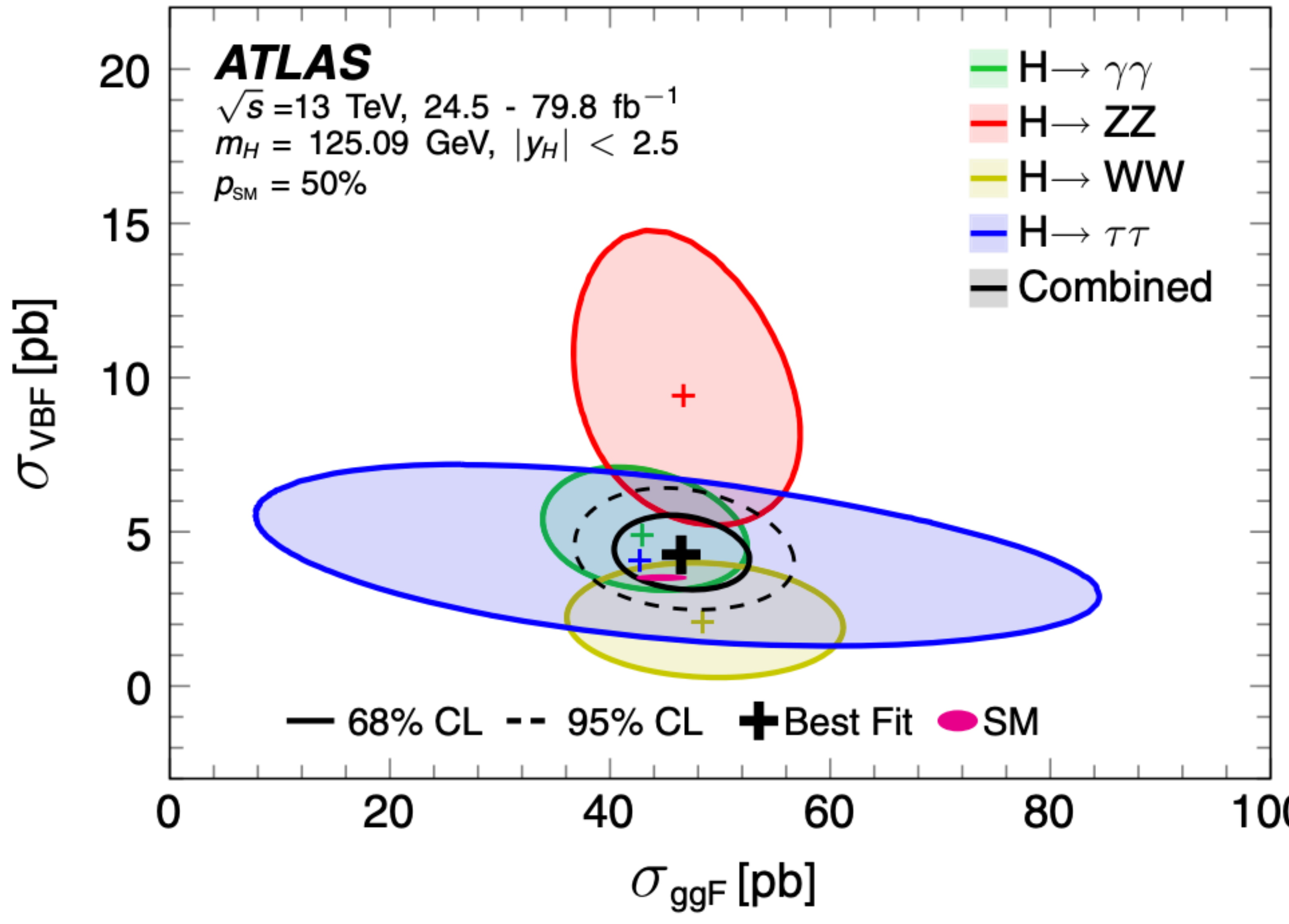

FIG. 4. Observed likelihood contours in the plane of σ_{VBF} versus σ_{ggF} from individual channels and the combined fit. Contours for 68% CL, defined in the asymptotic approximation by $-2\ln\Lambda = 2.28$, are shown as solid lines. The 95% CL contour for the combined fit, corresponding to $-2\ln\Lambda = 5.99$, is also shown as a dashed line. The crosses indicate the best-fit values, and the solid ellipse the SM prediction. Higgs boson branching fractions are fixed to their SM values within theory uncertainties. The probability of compatibility between the combined measurement and the SM prediction, estimated using the procedure outlined in the text with two d.o.f., corresponds to a p-value of $p_{SM} = 50\%$.

CMS

EPJC 79 (2019) 421

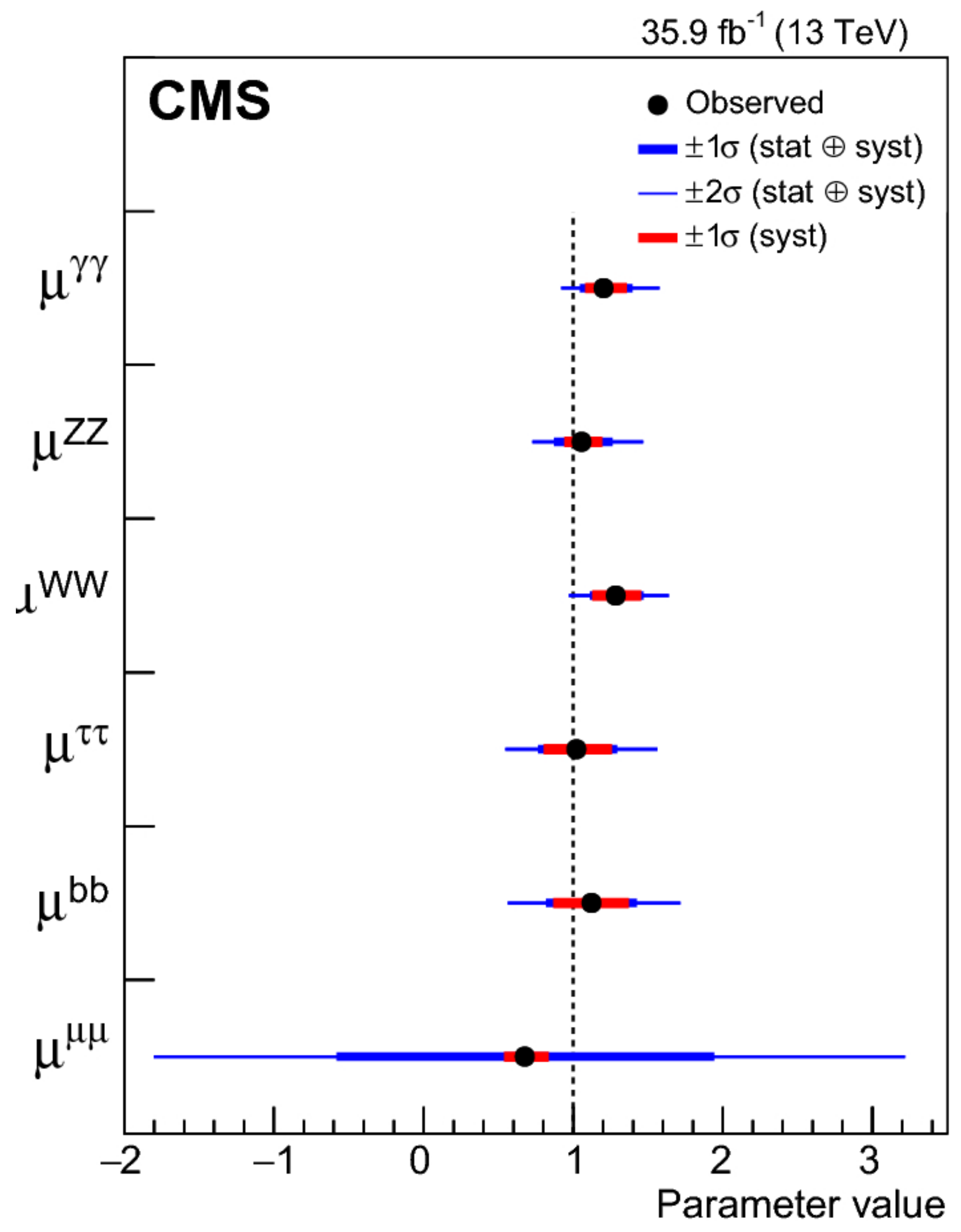

Higgs boson couplings: combined measurement

PRD 101 (2020) 012002 **ATLAS**

Production	Loops	Interference	Effective modifier	Resolved modifier
$\sigma(ggF)$	✓	t–b	κ_g^2	$1.04\,\kappa_t^2 + 0.002\,\kappa_b^2 - 0.04\,\kappa_t\kappa_b$
$\sigma(VBF)$	-	-	-	$0.73\,\kappa_W^2 + 0.27\,\kappa_Z^2$
$\sigma(qq/qg \to ZH)$	-	-	-	κ_Z^2
$\sigma(gg \to ZH)$	✓	t–Z	$\kappa_{(ggZH)}$	$2.46\,\kappa_Z^2 + 0.46\,\kappa_t^2 - 1.90\,\kappa_Z\kappa_t$
$\sigma(WH)$	-	-	-	κ_W^2
$\sigma(t\bar{t}H)$	-	-	-	κ_t^2
$\sigma(tHW)$	-	t–W	-	$2.91\,\kappa_t^2 + 2.31\,\kappa_W^2 - 4.22\,\kappa_t\kappa_W$
$\sigma(tHq)$	-	t–W	-	$2.63\,\kappa_t^2 + 3.58\,\kappa_W^2 - 5.21\,\kappa_t\kappa_W$
$\sigma(b\bar{b}H)$	-	-	-	κ_b^2
Partial decay width				
Γ^{bb}	-	-	-	κ_b^2
Γ^{WW}	-	-	-	κ_W^2
Γ^{gg}	✓	t–b	κ_g^2	$1.11\,\kappa_t^2 + 0.01\,\kappa_b^2 - 0.12\,\kappa_t\kappa_b$
$\Gamma^{\tau\tau}$	-	-	-	κ_τ^2
Γ^{ZZ}	-	-	-	κ_Z^2
Γ^{cc}	-	-	-	$\kappa_c^2\ (=\kappa_t^2)$
$\Gamma^{\gamma\gamma}$	✓	t–W	κ_γ^2	$1.59\,\kappa_W^2 + 0.07\,\kappa_t^2 - 0.67\,\kappa_W\kappa_t$
$\Gamma^{Z\gamma}$	✓	t–W	$\kappa_{(Z\gamma)}^2$	$1.12\,\kappa_W^2 - 0.12\,\kappa_W\kappa_t$
Γ^{ss}	-	-	-	$\kappa_s^2\ (=\kappa_b^2)$
$\Gamma^{\mu\mu}$	-	-	-	κ_μ^2
Total width ($B_{\rm inv} = B_{\rm undet} = 0$)				
Γ_H	✓	-	κ_H^2	$0.58\,\kappa_b^2 + 0.22\,\kappa_W^2$ $+0.08\,\kappa_g^2 + 0.06\,\kappa_\tau^2$ $+0.03\,\kappa_Z^2 + 0.03\,\kappa_c^2$ $+0.0023\,\kappa_\gamma^2 + 0.0015\,\kappa_{(Z\gamma)}^2$ $+0.0004\,\kappa_s^2 + 0.00022\,\kappa_\mu^2$

CMS EPJC 79 (2019) 421

An additional fit is performed using a phenomenological parametrization relating the masses of the fermions and vector bosons to the corresponding κ modifiers using two parameters, denoted M and ϵ [113, 114]. In such a model one can relate the coupling modifiers to M and ϵ as $\kappa_F = v\, m_f^{\epsilon}/M^{1+\epsilon}$ for fermions and $\kappa_V = v\, m_V^{2\epsilon}/M^{1+2\epsilon}$ for vector bosons. Here, $v = 246.22$ GeV, is the SM Higgs boson vacuum expectation value [115]. The SM expectation, $\kappa_i = 1$, is recovered when $(M, \epsilon) = (v, 0)$.

Effective	Loops	Interference	Scaling factor	Resolved scaling factor
Production				
σ(ggH)	✓	g-t	κ_g^2	$1.04\kappa_t^2 + 0.002\kappa_b^2 - 0.038\kappa_t\kappa_b$
σ(VBF)	—	—		$0.73\kappa_W^2 + 0.27\kappa_Z^2$
σ(WH)	—	—		κ_W^2
σ(qq/qg → ZH)	—	—		κ_Z^2
σ(gg → ZH)	✓	Z-t		$2.46\kappa_Z^2 + 0.47\kappa_t^2 - 1.94\kappa_Z\kappa_t$
σ(ttH)	—	—		κ_t^2
σ(gb → WtH)	—	W-t		$2.91\kappa_t^2 + 2.31\kappa_W^2 - 4.22\kappa_t\kappa_W$
σ(qb → tHq)	—	W-t		$2.63\kappa_t^2 + 3.58\kappa_W^2 - 5.21\kappa_t\kappa_W$
σ(bbH)	—	—		κ_b^2
Partial decay width				
Γ^{ZZ}	—	—		κ_Z^2
Γ^{WW}	—	—		κ_W^2
$\Gamma^{\gamma\gamma}$	✓	W-t	κ_γ^2	$1.59\kappa_W^2 + 0.07\kappa_t^2 - 0.67\kappa_W\kappa_t$
$\Gamma^{\tau\tau}$	—	—		κ_τ^2
Γ^{bb}	—	—		κ_b^2
$\Gamma^{\mu\mu}$	—	—		κ_μ^2
Total width for $\mathcal{B}_{\rm BSM} = 0$				
Γ_H	✓	—	κ_H^2	$0.58\kappa_b^2 + 0.22\kappa_W^2 + 0.08\kappa_g^2$ $+0.06\kappa_\tau^2 + 0.026\kappa_Z^2 + 0.029\kappa_c^2$ $+0.0023\kappa_\gamma^2 + 0.0015\kappa_{Z\gamma}^2$ $+0.00025\kappa_s^2 + 0.00022\kappa_\mu^2$

Higgs boson couplings: combined measurement

PRD 101 (2020) 012002

ATLAS

up to 79.8 fb^{-1}

$$H \to \gamma\gamma, ZZ^*, WW^*, \tau\tau, b\bar{b}, \mu\mu$$

CMS

35.9 fb^{-1}

EPJC 79 (2019) 421

Parameter	Result
κ_Z	1.10 ± 0.08
κ_W	1.05 ± 0.08
κ_b	$1.06\ ^{+\ 0.19}_{-\ 0.18}$
κ_t	$1.02\ ^{+\ 0.11}_{-\ 0.10}$
κ_τ	1.07 ± 0.15
κ_μ	< 1.53 at 95% CL

$\Gamma_{H,\,TOT}$ is affected both by modifications of the κ_j and contributions from two additional classes of Higgs boson decays

- invisible decays, which are identified through an E_T^{miss} signatures;
- undetected decays, to which none of the analyses included in this combination are sensitive;
- BR for decays into invisible final states is ~ 0.1%, from the H→ZZ*→4ν process
  - BSM contributions to these BRs are denoted by B_{inv} and B_{undet}.

Parameter	Best fit value	
κ_W	1.10	$^{+0.12}_{-0.17}$ $\left(^{+0.11}_{-0.10}\right)$
κ_Z	0.99	$^{+0.11}_{-0.12}$ $\left(^{+0.11}_{-0.11}\right)$
κ_t	1.11	$^{+0.12}_{-0.10}$ $\left(^{+0.11}_{-0.12}\right)$
κ_b	−1.10	$^{+0.33}_{-0.23}$ $\left(^{+0.22}_{-0.22}\right)$
κ_τ	1.01	$^{+0.16}_{-0.20}$ $\left(^{+0.17}_{-0.15}\right)$
κ_μ	0.79	$^{+0.58}_{-0.79}$ $\left(^{+0.50}_{-1.01}\right)$

Higgs boson cross-section measurement: differential

ATLAS-CONF-2019-032

ATLAS

139 fb^{-1}

$$H \to \gamma\gamma, ZZ^*$$

$p_{T,H}$ Bin	$d\sigma/dp_{T,H}$ (pb/GeV)
0-10 GeV	0.73 ± 0.15
10-20 GeV	1.16 ± 0.21
20-30 GeV	0.80 ± 0.15
30-45 GeV	0.58 ± 0.10
45-60 GeV	0.278 ± 0.075
60-80 GeV	0.215 ± 0.054
80-120 GeV	0.142 ± 0.023
120-200 GeV	0.044 ± 0.007
200-350 GeV	0.007 ± 0.001
350-1000 GeV	$0.0002 \pm 8 \times 10^{-5}$

35.9 fb^{-1}

CMS

PLB 792 (2019) 369

$$H \to \gamma\gamma, ZZ^*, b\bar{b}$$

Channel	p_T^H binning (GeV)								
$H \to \gamma\gamma$	[0, 15)	[15, 30)	[30, 45)	[45, 80)	[80, 120)	[120, 200)	[200, 350)	[350, 600)	[600, ∞)
$H \to ZZ$	[0, 15)	[15, 30)	[30, 80)		[80, 200)		[200, ∞)		
$H \to b\bar{b}$	None							[350, 600)	[600, ∞)

Channel	N_{jets} binning				
$H \to \gamma\gamma$	0	1	2	3	≥ 4
$H \to ZZ$	0	1	2	≥ 3	

Channel	$\lvert y_H \rvert$ binning					
$H \to \gamma\gamma$	[0.0, 0.15)	[0.15, 0.30)	[0.30, 0.60)	[0.60, 0.90)	[0.90, 1.20)	[1.20, 2.50]
$H \to ZZ$	[0.0, 0.15)	[0.15, 0.30)	[0.30, 0.60)	[0.60, 0.90)	[0.90, 1.20)	[1.20, 2.50]

Channel	p_T^{jet} binning (GeV)					
$H \to \gamma\gamma$	[0, 30)	[30, 55)	[55, 95)	[95, 120)	[120, 200)	[200, ∞)
$H \to ZZ$	[0, 30)	[30, 55)	[55, 95)	[95, ∞)		

$$\mathcal{L}(\vec{\Delta\sigma}\,|\vec{\theta}) = \prod_{m=1}^{n_c} \mathcal{L}_m(\vec{\Delta\sigma}\,|\vec{\theta})\,\mathrm{pdf}(\vec{\theta})$$

Higgs boson cross-section measurement: differential

35.9 fb^{-1}

CMS

PLB 792 (2019) 369

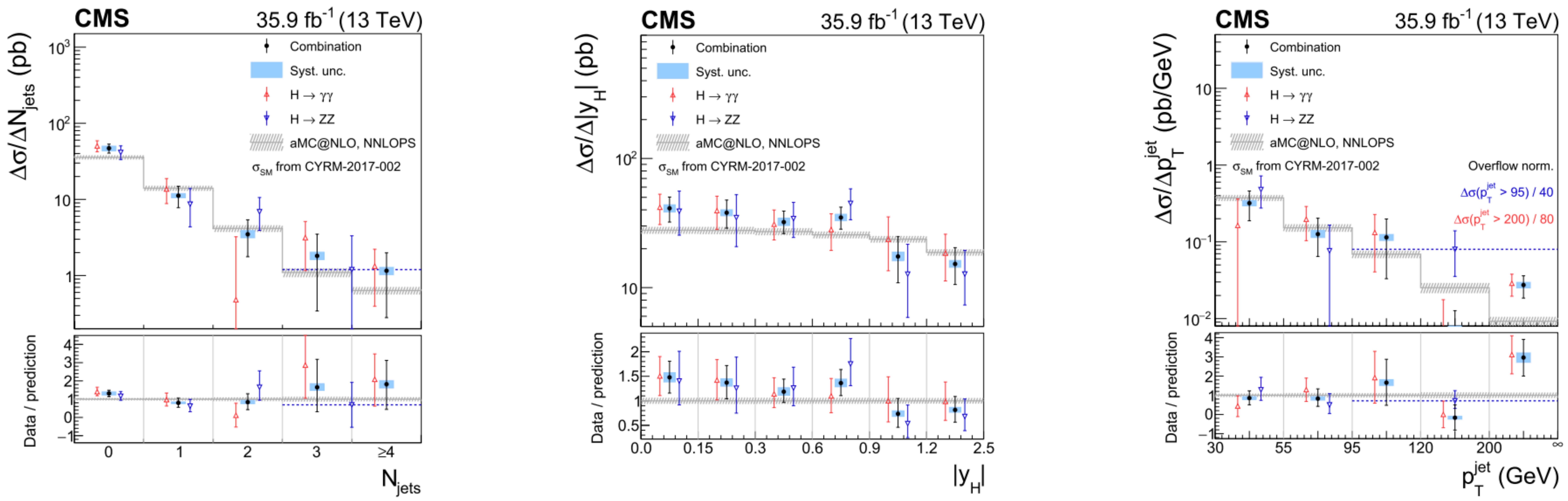

Higgs boson width measurement: constraints

[PLB 786 (2018) 223-244](#) **ATLAS** **36 fb^{-1}**

24.8 fb^{-1}+80.2 fb^{-1} **CMS** [JHEP 11 (2017) 047](#)

$H \to ZZ^* \to 4l\,/\,2l2\nu$ $\quad H \to ZZ \to 4l\,/\,2l2\nu$

$$m_T^{ZZ} = \sqrt{\left[\sqrt{m_Z^2 + (p_T^{ll})^2} + \sqrt{m_Z^2 + (E_T^{\rm miss})^2}\right]^2 - |\vec{p}_T^{\,ll} + \vec{E}_T^{\rm miss}|^2}$$

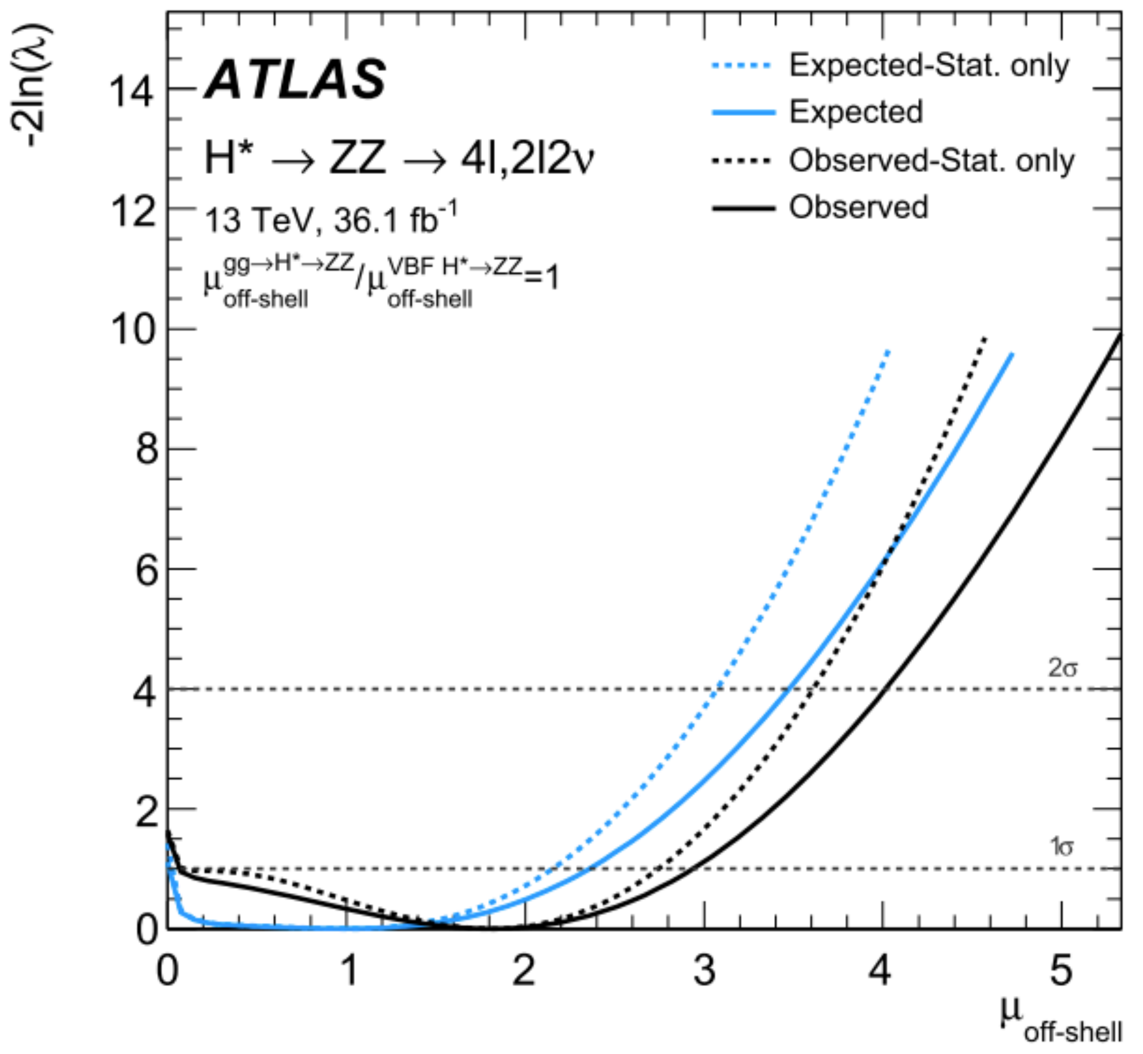

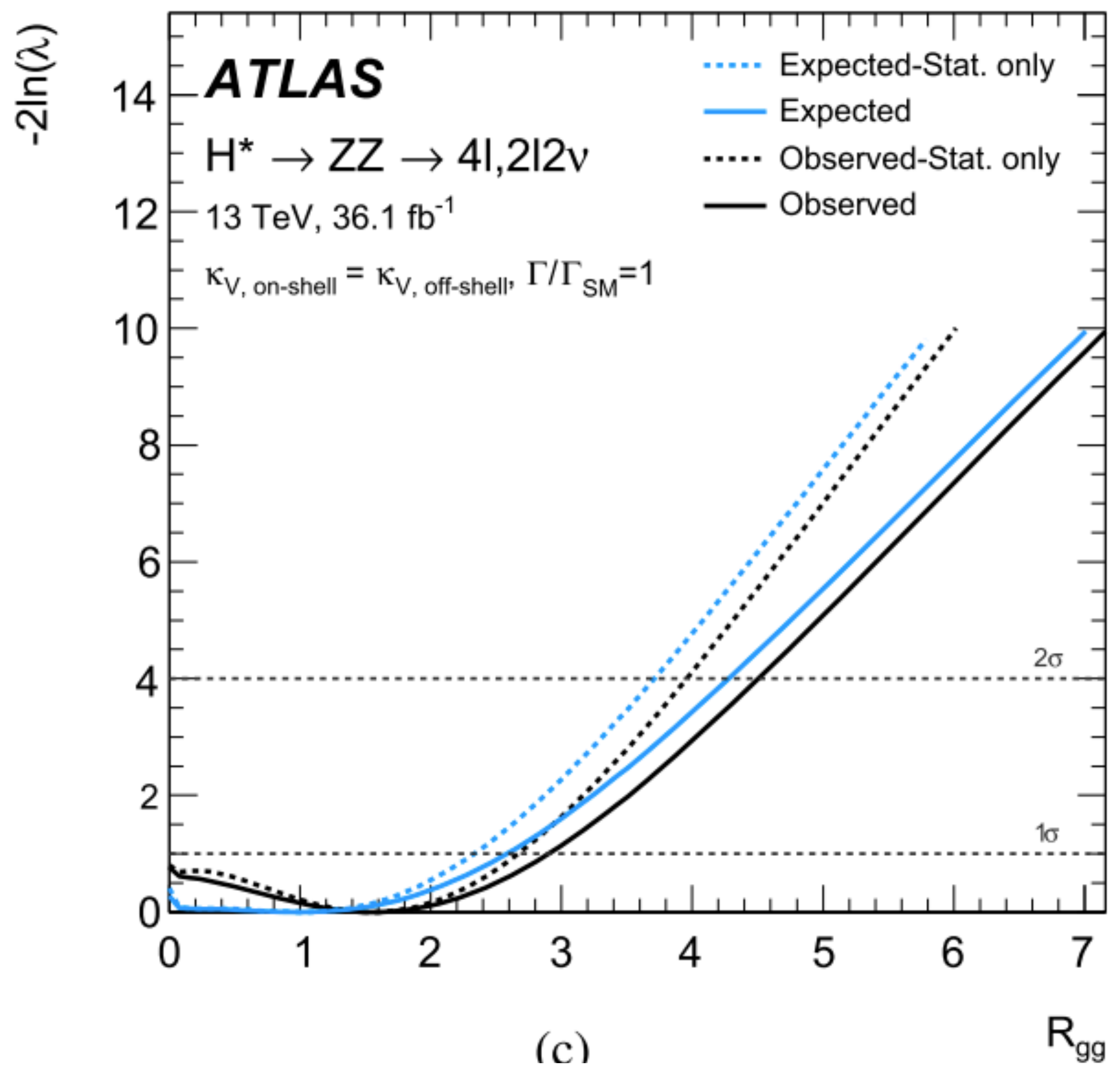

		Observed	Expected		
			Median	$\pm 1\ \sigma$	$\pm 2\ \sigma$
$\mu_{\text{off-shell}}$	$ZZ \to 4\ell$ analysis	4.5	4.3	[3.3, 5.4]	[2.7, 7.1]
	$ZZ \to 2\ell 2\nu$ analysis	5.3	4.4	[3.4, 5.5]	[2.8, 7.0]
	Combined	3.8	3.4	[2.7, 4.2]	[2.3, 5.3]
$\Gamma_H/\Gamma_H^{\rm SM}$	Combined	3.5	3.7	[2.9, 4.8]	[2.4, 6.5]
R_{gg}	Combined	4.3	4.1	[3.3, 5.6]	[2.7, 8.2]

$H \to ZZ^* \to 4l$ $\quad H \to ZZ \to 4l$

Parameter	Observed	Expected
Γ_H (MeV)	$3.2^{+2.8}_{-2.2}$ [0.08, 9.16]	$4.1^{+5.0}_{-4.0}$ [0.0, 13.7]

$$R_{gg} = k^2_{g,\text{off-shell}} / k^2_{g,\text{on-shell}}$$

Higgs boson width measurement: constraints

PLB 786 (2018) 223-244

ATLAS

36 fb^{-1}

$H \rightarrow ZZ^* \rightarrow 4l\,/\,2l2\nu$ $\quad H \rightarrow ZZ \rightarrow 4l\,/\,2l2\nu$

Systematic uncertainty	95% CL upper limit on $\mu_{\text{off-shell}}$		
	$ZZ \rightarrow 4\ell$	$ZZ \rightarrow 2\ell 2\nu$	Combined
QCD scale $q\bar{q} \rightarrow ZZ$	4.2	3.9	3.2
QCD scale $gg \rightarrow (H^* \rightarrow) ZZ$	4.2	3.6	3.1
Luminosity	4.1	3.5	3.1
Remaining systematic uncertainties	4.1	3.5	3.0
All systematic uncertainties	4.3	4.4	3.4
No systematic uncertainties	4.0	3.4	3.0

24.8 fb^{-1}+80.2 fb^{-1}

CMS

JHEP 11 (2017) 047

$H \rightarrow ZZ^* \rightarrow 4l$ $\quad H \rightarrow ZZ \rightarrow 4l$

Search for H → μμ decay mode

ATLAS — 139 fb^{-1}

PLB 784 (2018) 345

Category	0-jet	1-jet	VBF	2-jet $O_{\mathrm{VBF}} < 0.60$
High	$O^0_{ggF} \geq 0.75$	$O^1_{ggF} \geq 0.78$	$O_{\mathrm{VBF}} \geq 0.89$	$O^2_{ggF} \geq 0.48$
Medium	$0.35 \leq O^0_{ggF} < 0.75$	$0.38 \leq O^1_{ggF} < 0.78$	$0.77 \leq O_{\mathrm{VBF}} < 0.89$	$0.22 \leq O^2_{ggF} < 0.48$
Low	$O^0_{ggF} < 0.35$	$O^1_{ggF} < 0.38$	$0.60 \leq O_{\mathrm{VBF}} < 0.77$	$O^2_{ggF} < 0.22$

Category	Data	S_{SM}	S	B	$S/\sqrt{B}$	S/B [%]
VBF High	40	4.5	2.3	34	0.39	6.6
VBF Medium	109	5.5	2.8	100	0.28	2.8
VBF Low	450	9.6	4.9	420	0.24	1.2
2-jet High	3400	38	19	3440	0.33	0.6
2-jet Medium	13938	70	35	13910	0.30	0.3
2-jet Low	40747	75	38	40860	0.19	0.1
1-jet High	2885	32	16	2830	0.31	0.6
1-jet Medium	24919	107	54	24890	0.35	0.2
1-jet Low	77482	134	68	77670	0.24	0.1
0-jet High	24777	85	43	24740	0.27	0.2
0-jet Medium	85281	155	79	85000	0.27	0.1
0-jet Low	180478	144	73	180000	0.17	<0.1

CMS — 35.9 fb^{-1}

JHEP 11 (2017) 047

BDT response quantile (%)	Maximum muon $\|\eta\|$	ggH (%)	VBF (%)	WH (%)	ZH (%)	$t\bar{t}H$ (%)	Signal	Bkg/GeV @125 GeV	FWHM (GeV)	Bkg fit function	$S/\sqrt{B}$ @ FWHM
0–8	$\|\eta\| < 2.4$	4.9	1.3	3.3	6.3	32	21.2	3.13×10^3	4.2	$\mathcal{D}_{\mathrm{MBW}}\ B_{\mathrm{deg}\ 4}$	0.12
8–39	$1.9 < \|\eta\| < 2.4$	5.6	1.7	3.9	3.5	1.3	22.3	1.34×10^3	7.2	$\mathcal{D}_{\mathrm{MBW}}\ B_{\mathrm{deg}\ 4}$	0.16
8–39	$0.9 < \|\eta\| < 1.9$	10	2.8	6.5	6.4	5.2	41.1	2.24×10^3	4.1	$\mathcal{D}_{\mathrm{MBW}}\ B_{\mathrm{deg}\ 4}$	0.29
8–39	$\|\eta\| < 0.9$	3.2	0.8	1.9	2.1	3.5	12.7	7.83×10^2	2.9	$\mathcal{D}_{\mathrm{MBW}}\ B_{\mathrm{deg}\ 4}$	0.18
39–61	$1.9 < \|\eta\| < 2.4$	2.9	1.7	2.7	2.7	0.3	11.8	4.37×10^2	7.0	$\mathcal{D}_{\mathrm{MBW}}\ B_{\mathrm{deg}\ 4}$	0.14
39–61	$0.9 < \|\eta\| < 1.9$	7.2	3.3	6.1	5.2	1.3	29.2	9.70×10^2	4.0	$\mathcal{D}_{\mathrm{MBW}}\ B_{\mathrm{deg}\ 4}$	0.31
39–61	$\|\eta\| < 0.9$	3.6	1.1	2.6	2.2	0.9	14.5	4.81×10^2	2.8	$\mathcal{D}_{\mathrm{MBW}}$	0.26
61–76	$1.9 < \|\eta\| < 2.4$	1.2	1.5	1.8	1.7	0.2	5.2	1.48×10^2	7.6	$\mathcal{D}_{\mathrm{MBW}}\ B_{\mathrm{deg}\ 4}$	0.11
61–76	$0.9 < \|\eta\| < 1.9$	4.8	3.6	4.5	4.4	0.7	20.3	5.12×10^2	4.2	$\mathcal{D}_{\mathrm{MBW}}\ B_{\mathrm{deg}\ 4}$	0.29
61–76	$\|\eta\| < 0.9$	3.2	1.6	2.3	2.1	0.6	13.1	3.22×10^2	3.0	$\mathcal{D}_{\mathrm{MBW}}$	0.28
76–91	$1.9 < \|\eta\| < 2.4$	1.2	3.1	2.2	2.1	0.2	5.8	1.04×10^2	7.1	$\mathcal{D}_{\mathrm{MBW}}\ B_{\mathrm{deg}\ 4}$	0.14
76–91	$0.9 < \|\eta\| < 1.9$	4.4	8.7	6.2	6.0	1.1	20.3	3.60×10^2	4.2	$\mathcal{D}_{\mathrm{MBW}}\ B_{\mathrm{deg}\ 4}$	0.35
76–91	$\|\eta\| < 0.9$	3.1	4.0	3.8	3.6	0.9	13.7	2.36×10^2	3.2	$\mathcal{D}_{\mathrm{MBW}}$	0.34
91–95	$\|\eta\| < 2.4$	1.7	6.4	2.5	2.6	0.5	8.6	96.0	4.0	$\mathcal{D}_{\mathrm{MBW}}$	0.28
95–100	$\|\eta\| < 2.4$	2.0	19	1.5	1.4	0.7	13.7	83.4	4.1	$\mathcal{D}_{\mathrm{MBW}}$	0.48
Total	$\|\eta\| < 2.4$	59	61	51	52	49	253	1.30×10^4	3.9		

Higgs self-coupling constraints

ATLAS only ATL-PHYS-PUB-2019-009

$H \to \gamma\gamma, ZZ^*, WW^*, \tau\tau, b\bar{b}, \mu\mu$

up to 79.8 fb^{-1}

Analysis	Integrated luminosity (fb^{-1})
$H \to \gamma\gamma$ (including $t\bar{t}H$, $H \to \gamma\gamma$)	79.8
$H \to ZZ^* \to 4\ell$ (including $t\bar{t}H$, $H \to ZZ^* \to 4\ell$)	79.8
$H \to WW^* \to e\nu\mu\nu$	36.1
$H \to \tau\tau$	36.1
VH, $H \to b\bar{b}$	79.8
$t\bar{t}H$, $H \to b\bar{b}$ and $t\bar{t}H$ multilepton	36.1

	$H \to \gamma\gamma$	$H \to ZZ^*$	$H \to WW^*$	$H \to \tau\tau$	$H \to b\bar{b}$
$t\bar{t}H$	$t\bar{t}H$ leptonic (3 categories) $t\bar{t}H$ hadronic (4 categories)	$t\bar{t}H$ multilepton 1 ℓ + 2 τ_{had} $t\bar{t}H$ multilepton 2 opposite-sign ℓ + 1 τ_{had} $t\bar{t}H$ multilepton 2 same-sign ℓ (categories for 0 or 1 τ_{had}) $t\bar{t}H$ multilepton 3 ℓ (categories for 0 or 1 τ_{had}) $t\bar{t}H$ multilepton 4 ℓ (except $H \to ZZ^* \to 4\ell$) $t\bar{t}H$ leptonic, $H \to ZZ^* \to 4\ell$ $t\bar{t}H$ hadronic, $H \to ZZ^* \to 4\ell$			$t\bar{t}H$ 1 ℓ, boosted $t\bar{t}H$ 1 ℓ, resolved (11 categories) $t\bar{t}H$ 2 ℓ (7 categories)
VH	VH 2 ℓ VH 1 ℓ, $p_T^{\ell+E_T^{miss}} \geq 150$ GeV VH 1 ℓ, $p_T^{\ell+E_T^{miss}} < 150$ GeV VH E_T^{miss}, $E_T^{miss} \geq 150$ GeV VH E_T^{miss}, $E_T^{miss} < 150$ GeV VH+VBF $p_T^{j1} \geq 200$ GeV VH hadronic (2 categories)	VH leptonic 0-jet, $p_T^{4\ell} \geq 100$ GeV 2-jet, $m_{jj} < 120$ GeV			2 ℓ, $75 \leq p_T^V < 150$ GeV, $N_{jets} = 2$ 2 ℓ, $75 \leq p_T^V < 150$ GeV, $N_{jets} \geq 3$ 2 ℓ, $p_T^V \geq 150$ GeV, $N_{jets} = 2$ 2 ℓ, $p_T^V \geq 150$ GeV, $N_{jets} \geq 3$ 1 ℓ $p_T^V \geq 150$ GeV, $N_{jets} = 2$ 1 ℓ $p_T^V \geq 150$ GeV, $N_{jets} = 3$ 0 ℓ, $p_T^V \geq 150$ GeV, $N_{jets} = 2$ 0 ℓ, $p_T^V \geq 150$ GeV, $N_{jets} = 3$
VBF	VBF, $p_T^{\gamma\gamma jj} \geq 25$ GeV (2 categories) VBF, $p_T^{\gamma\gamma jj} < 25$ GeV (2 categories)	2-jet VBF, $p_T^{j1} \geq 200$ GeV 2-jet VBF, $p_T^{j1} < 200$ GeV	2-jet VBF	VBF $p_T^{\tau\tau} > 140$ GeV ($\tau_{had}\tau_{had}$ only) VBF high-m_{jj} VBF low-m_{jj}	
ggF	2-jet, $p_T^{\gamma\gamma} \geq 200$ GeV 2-jet, 120 GeV $\leq p_T^{\gamma\gamma} < 200$ GeV 2-jet, 60 GeV $\leq p_T^{\gamma\gamma} < 120$ GeV 2-jet, $p_T^{\gamma\gamma} < 60$ GeV 1-jet, $p_T^{\gamma\gamma} \geq 200$ GeV 1-jet, 120 GeV $\leq p_T^{\gamma\gamma} < 200$ GeV 1-jet, 60 GeV $\leq p_T^{\gamma\gamma} < 120$ GeV 1-jet, $p_T^{\gamma\gamma} < 60$ GeV 0-jet (2 categories)	1-jet, $p_T^{4\ell} \geq 120$ GeV 1-jet, 60 GeV $\leq p_T^{4\ell} < 120$ GeV 1-jet, $p_T^{4\ell} < 60$ GeV 0-jet, $p_T^{4\ell} < 100$ GeV	1-jet, $m_{\ell\ell} < 30$ GeV, $p_T^{\ell_2} < 20$ GeV 1-jet, $m_{\ell\ell} < 30$ GeV, $p_T^{\ell_2} \geq 20$ GeV 1-jet, $m_{\ell\ell} \geq 30$ GeV, $p_T^{\ell_2} < 20$ GeV 1-jet, $m_{\ell\ell} \geq 30$ GeV, $p_T^{\ell_2} \geq 20$ GeV 0-jet, $m_{\ell\ell} < 30$ GeV, $p_T^{\ell_2} < 20$ GeV 0-jet, $m_{\ell\ell} < 30$ GeV, $p_T^{\ell_2} \geq 20$ GeV 0-jet, $m_{\ell\ell} \geq 30$ GeV, $p_T^{\ell_2} < 20$ GeV 0-jet, $m_{\ell\ell} \geq 30$ GeV, $p_T^{\ell_2} \geq 20$ GeV	Boosted, $p_T^{\tau\tau} > 140$ GeV Boosted, $p_T^{\tau\tau} \leq 140$ GeV	

Higgs self-coupling constraints

ATLAS only ATL-PHYS-PUB-2019-009

$$H \to \gamma\gamma, ZZ^*, WW^*, \tau\tau, b\bar{b}, \mu\mu$$

up to 79.8 fb^{-1}

$$\mu_i(\kappa_\lambda, \kappa_i) = \frac{\sigma^{\rm BSM}}{\sigma^{\rm SM}} = Z_H^{\rm BSM}(\kappa_\lambda)\left[\kappa_i^2 + \frac{(\kappa_\lambda - 1)C_1^i}{K_{\rm EW}^i}\right]$$

$$\mu_f(\kappa_\lambda, \kappa_f) = \frac{{\rm BR}_f^{\rm BSM}}{{\rm BR}_f^{SM}} = \frac{\kappa_f^2 + (\kappa_\lambda - 1)C_1^f}{\sum_j {\rm BR}_j^{\rm SM}\left[\kappa_j^2 + (\kappa_\lambda - 1)C_1^j\right]}$$

accounting for effect due to the variation of the trilinear coupling λ_{HHH}: both production cross section and BRs.

Figure 2: Variation of the cross-sections (a) and branching fractions (b) as a function of the trilinear coupling modifier κ_λ. The plots represent the equations (2) and (4) using the numerical values shown in Tables 3 and 4, all obtained

$$Z_H^{\rm BSM}(\kappa_\lambda) = \frac{1}{1 - (\kappa_\lambda^2 - 1)\delta Z_H} \quad \text{with} \quad \delta Z_H = -1.536 \times 10^{-3}$$